952184 N.I. 68-

Report No. TE 4092/3-183-68

Thermo Electron Corporation, 85 First Avenue, Waltham, Massachusetts 02154

SECOND QUARTERLY PROGRESS REPORT

APPLIED THERMIONIC RESEARCH

Contract 952184

4 March 1968 to 4 June 1968

E. P. Gyftopoulos, G. N. Hatsopoulos
F. Holly, D. Lieb, F. Rufeh, M. Shaw,
L. van Someren and C. Wang

Prepared for

Jet Propulsion Laboratory
Pasadena, California

Report No. TE 4092/3-183-68

Thermo Electron Corporation, 85 First Avenue, Waltham, Massachusetts 02154

SECOND QUARTERLY PROGRESS REPORT

APPLIED THERMIONIC RESEARCH

Contract 952184

4 March 1968 to 4 June 1968

E. P. Gyftopoulos, G. N. Hatsopoulos
F. Holly, D. Lieb, F. Rufeh, M. Shaw,
L. van Someren and C. Wang

Prepared for

Jet Propulsion Laboratory
Pasadena, California

This work was performed for the Jet Propulsion Laboratory, California Institute of Technology, sponsored by the National Aeronautics and Space Administration under Contract NAS7-100.

This report contains information prepared by Thermo Electron Corporation under JPL subcontract. Its content is not necessarily endorsed by the Jet Propulsion Laboratory, California Institute of Technology, or the National Aeronautics and Space Administration.

TABLE OF CONTENTS

TABLE OF CONTENTS (continued)

CHAPTER I

INTRODUCTION AND SUMMARY

Thermochemical data were obtained on the oxidation products of cesium by differential thermal analysis (Chapter II). A rather complex mixture was obtained and peaks which could be attributable to Cs_3O, CsOH and Cs_2O_3 were observed. Presumably, Cs_2O was present as well, but it could not be identified because it has no reported transition points in the temperature range of the experiment. The mass spectrometer system was checked out using nitrogen for the purpose of estimating requirements for the signal detection scheme. A Knudsen cell has been built and tried out on the system with pure cesium in order to develop procedures for handling cesium in the system. Vapor pressure curves for cesium were taken.

Rigorous definitions are given of electronegativity of atoms, neutral or ionized, and of atomic orbitals (Chapter III). The definitions are consistent with the rules of the statistics of ensembles and the quantum-mechanical picture of atomic species.

A variable-spacing, guard-ring converter with a single-crystal tungsten emitter and a molybdenum collector was constructed during the first quarter. Experimental data from this converter, covering a wide range of emitter temperatures and interelectrode spacings, were presented in the First Quarterly Progress Report. During the second quarter, testing was completed and the data was used to study the dependence of the internal voltage drop on ion richness, β, and on cesium pressure, P, at constant values of Pd, where d is the interelectrode

spacing (Chapter IV). The preliminary results suggest that the voltage drop is a decreasing function of cesium pressure at constant values of Pd and β, and a decreasing function of β at constant values of P and d. A variable-spacing, guard-ring converter with a fluoride vapor-deposited tungsten emitter and a molybdenum collector was constructed in order to obtain data for comparison with in-pile test converters. Performance maps will be recorded shortly.

Further studies were made on the microstructure and preferred orientation of vapor-deposited tungsten emitters after exposure to various heat treatments in a vacuum (Chapter V). Heat treatment causes changes in the microstructure which are not necessarily accompanied by changes in the pole figure.

CHAPTER II

ELECTRONEGATIVE ADDITIVES

F. J. Holly and M. Shaw

A. THERMODYNAMICS OF CESIUM-OXYGEN SYSTEMS

Since cesium is an essential part of thermionic converters, it would be highly desirable if some oxide of cesium could be used as a source of continuous oxygen supply.

The cesium-oxygen system is complex. In the presence of excess cesium, several suboxides form, such as Cs_7O, Cs_4O, Cs_3O and Cs_7O_2.

When cesium is exposed to an excess of oxygen at room temperature, several oxides form: Cs_2O, Cs_2O_2, Cs_2O_3, and CsO_2. When heated, the higher oxides decompose to Cs_2O and oxygen (Table II-1).

Cesium oxide, Cs_2O, is relatively stable at higher temperatures. By considering the following equilibrium:

$$Cs_2O_{(s)} \rightleftarrows 2\,Cs_{(g)} + \frac{1}{2}\,O_{2(g)}$$

it is possible to calculate that, at cesium pressures of a few torr, such as exist in diodes, the equilibrium partial pressure of oxygen is

$$10^{-35} \text{ torr at } 575°K$$

and

$$10^{-8} \text{ torr at } T = 900°K$$

Therefore, it was suggested several years ago that solid cesium oxide could be considered as an oxygen source. However, it was shown in

TABLE II-1

OXIDATION OF CESIUM

T_{system}: 298°K POSSIBLE REACTIONS	$\Delta F°$ (298°K)* kcal/mole	EQUILIBRIUM P_{O_2} (298°K) torr
1. $14\,Cs(s) + O_2(g) = 2\,Cs_7O\,(\ell)$	< -132	$< 10^{-92}$
2. $8\,Cs(s) + O_2(g) = 2\,Cs_4O\,(\ell)$	< -132	$< 10^{-92}$
3. $6\,Cs(s) + O_2(g) = 2\,Cs_3O\,(s)$	< -132	$< 10^{-92}$
4. $7\,Cs(s) + O_2(g) = Cs_7O_2\,(s)$	< -132	$< 10^{-92}$
	P_{O_2} (initial): 1 torr ΔF kcal	
5. $2\,Cs(s) + 1/2\,O_2(g) = Cs_2O(s)$	-63.6	6×10^{-92}
6. $2\,Cs(s) + O_2(g) = Cs_2O_2(s)$	-76.9	2×10^{-55}
7. $Cs(s) + 3/2\,O_2(g) = Cs_2O_3(s)$	-84.3	2×10^{-40}
8. $2Cs(s) + O_2(g) = CsO_2(s)$	-47.8	2×10^{-34}

*Obtained from Reference 3

several experiments that cesium oxide volatilized at temperatures much lower than 900°K. Hence, either the free energy data was grossly in error, or molecular sublimation occurred at a rather low temperature.

Practically no experimental data are available on the vapor pressure of cesium oxides except one recent paper,[1] which mentions that at 620°K the vapor pressure of Cs_2O is approximately 10^{-3} torr. This contrasts sharply with the earlier predictions of Brewer.[2] Assuming that the Cs_2O volatilizes as the molecule, the following reaction has to be considered at the emitter:

$$Cs_2O_{(g)} \rightleftarrows 2\,Cs_{(g)} + \frac{1}{2}O_{2(g)} \qquad \Delta F^\circ_g(T)$$

The standard free energy of decomposition is known only for the reaction:

$$Cs_2O_{(\ell)} \rightleftarrows 2\,Cs_{(g)} + \frac{1}{2}O_{2(g)} \qquad \Delta F^\circ_\ell(T)$$

which is given by the following series:

$$\Delta F^\circ_\ell(T) = 113,790 + 23.03\,T \log T - 145.60T$$

It can be roughly estimated that the boiling point of the liquid Cs_2O is about 1300°K, so that its vapor pressure at 2000°K could be as high as 15,000 torr. This approximate value can be used to estimate $\Delta F^\circ_g(2000°K)$:

$$\Delta F^\circ_g(2000°K) = \Delta F^\circ_\ell(2000°K) + R\,T \ln P_{Cs_2O}$$

$$\Delta F^\circ_g(2000°K) \simeq -13,482 \text{ cals}$$

$$K(2000\,^{\circ}K) = \frac{P_{O_2}^{1/2} \cdot P_{Cs}^{2}}{P_{Cs_2O}} = 6.1 \times 10^{5} \text{ torr}^{3/2}$$

Assuming that the cesium pressure is 10 torr in the interelectrode spacing, a cesium oxide pressure as low as 2×10^{-8} torr would yield 10^{-8} torr of oxygen at the emitter at 2000°K.

Figure II-1 shows the predicted dissociation curve of Cs_2O vapor at 2000°K as a function of the solid oxide temperature. The vapor pressure of the cesium oxide at various temperatures is roughly estimated. It is conceivable that at temperatures as low as 400°K the vapor pressure of Cs_2O might be high enough to provide adequate oxygen coverage for the emitter.

Alternatively, other oxides of cesium are known to be present and might contribute to the release of oxygen. The following experiments were initiated in order to resolve these questions.

B. DIFFERENTIAL THERMAL ANALYSIS OF CESIUM OXIDES

We have used differential thermal analysis to obtain information on the oxides formed when cesium is exposed to oxygen at room temperature and at elevated temperatures.

Differential thermal analysis (DTA) is an analytical technique for studying the physical and chemical changes taking place in materials during heating or cooling. These changes generally involve either the liberation or absorption of heat and include crystal transitions, changes of state, decomposition and chemical reactions.

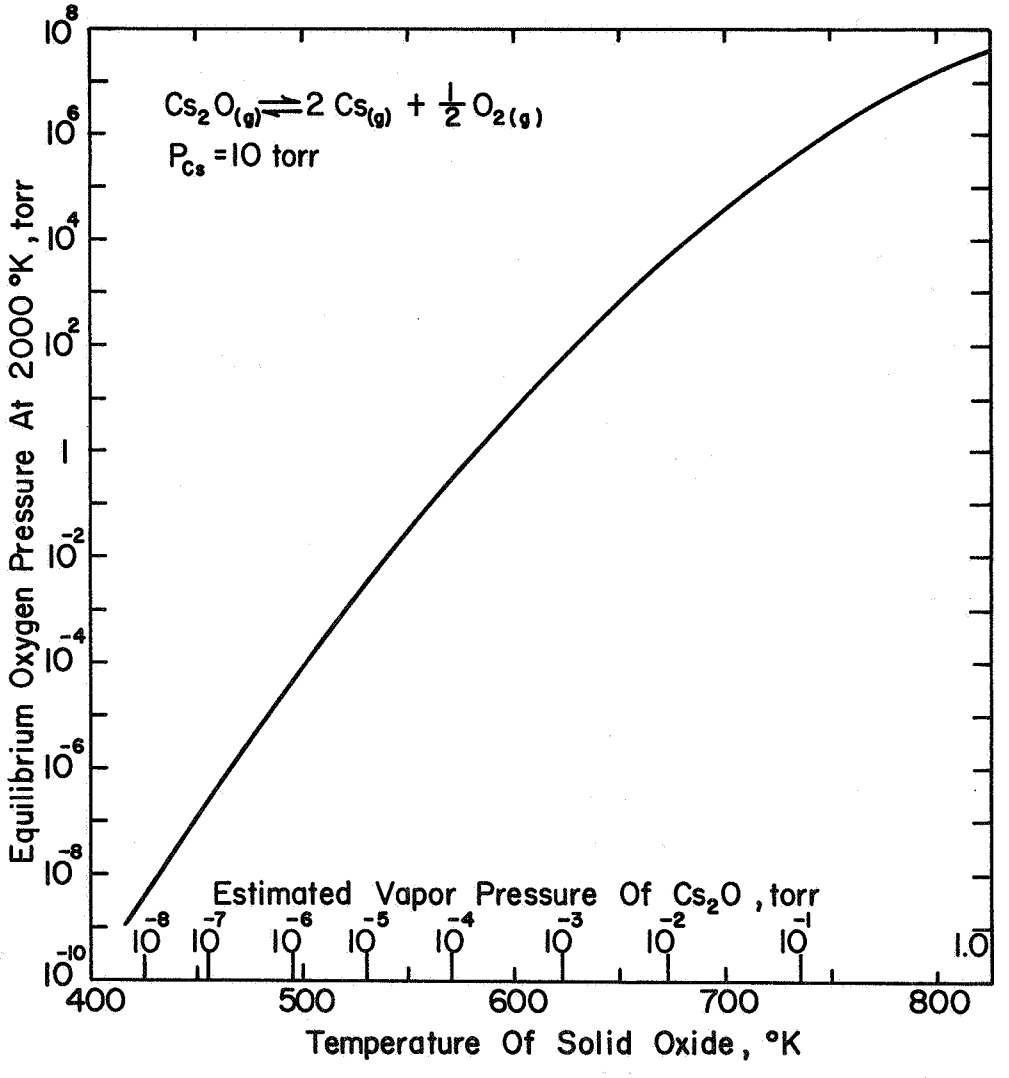

Figure II-1. Dissociation Curve of Cs_2O Vapor.

The technique of DTA involves continuous measurement of the temperature difference between a sample and a thermally inert reference material while both are heated at a given rate. A temperature difference will be measured between the sample and the reference only when the sample undergoes a physical or chemical change involving change of enthalpy. The sample temperature will lap behind the reference temperature during endothermic reactions and will exceed it during exothermic reactions.

When the temperature difference between the sample and the reference material is plotted as a function of increasing temperature, a curve known as a thermogram is produced. At temperatures where no physical or chemical changes are occurring in a sample, a straight baseline is produced. Peaks or deflections above the baseline represent exothermic reactions; peaks below the baseline represent endothermic reactions.

1. Modified DTA Apparatus

A rather complicated vacuum-tight holder connected to an oxygen measuring and feeding device and to a vacuum system was assembled last quarter and described in detail in the First Quarterly Report in order to study the thermal behavior of the cesium oxides. Difficulties associated both with the transport of cesium and with the stability of the reference junction were encountered. The use of such a device was abandoned in favor of placing the entire apparatus in a " dry box" which could be evacuated and the atmosphere controlled.

2. Dry Box Approach

The original open sample holder of the Fisher 210 Thermalyzer was used for the analysis. The furnace and the control system were

placed in a vacuum chamber equipped with rubber gloves. The reference material was dry alumina. The whole chamber was evacuated and then flushed with dry argon. This procedure was repeated two more times. Then a half-gram cesium capsule was broken, the metal was melted by body heat through the rubber gloves and glass, and some of the metal was transferred into the quartz tube sample holder. For the first run a chromel-alumel thermocouple was used; for all the other runs iron-constantan thermocouples were used.

In order to check the system, the temperature difference was recorded as a function of time while the metal was cooling down. An exothermic peak was obtained when the metal solidified (Figure II-2). Then the temperature of the furnace was increased at a constant rate of 10°C/min. A sharp exothermic peak a few degrees above room temperature indicated the melting of cesium (Figure II-2).

After cooling to room temperature, an oxygen-argon mixture was admitted to the system (~ 10 volume % O_2) while the temperature of the cesium sample was recorded. This temperature slowly increased during the next twenty minutes, then slowly decreased again due to the decreasing rate of oxidation which was due to external oxide layers (Figure II-3). The oxidation was accelerated by slow heating to 300°K in the presence of an O_2-Ar atmosphere.

The oxide mixture was thermo-analyzed. An endothermic peak was observed somewhat below 200°C, which may have been due to the melting of suboxide, Cs_3O.[3] Above 200°C some water bound to the hydroxide may have been lost, as evidenced by a broad endothermic peak. At 270°C, a well defined endothermic peak indicated the melting of CsOH[4] (Figure II-4).

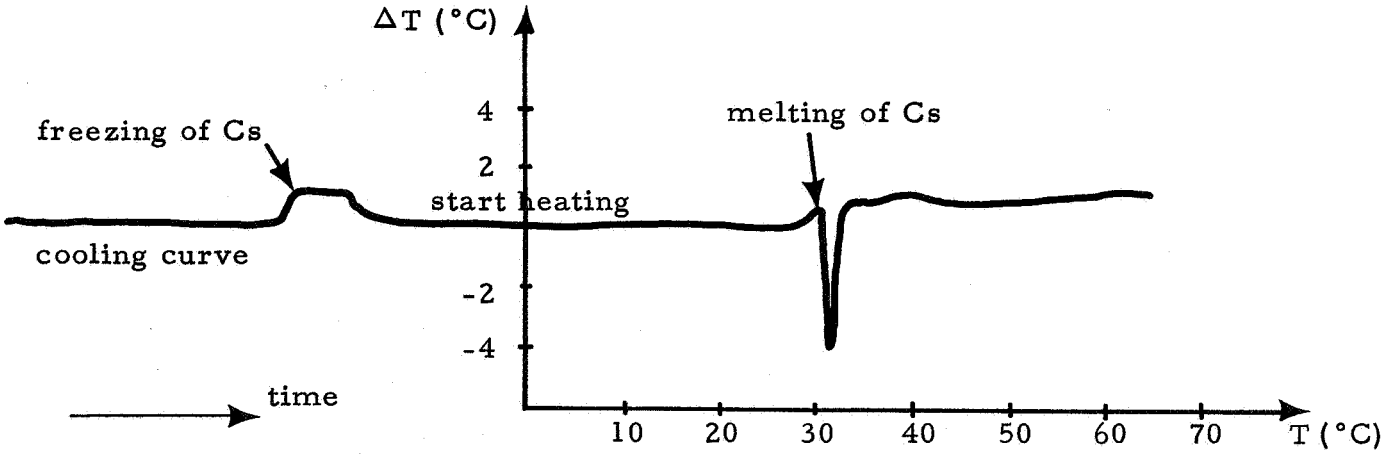

Figure II-2. Cooling and Heating Curve of Cesium Metal as Measured by the Fisher 210 Thermalyzer.

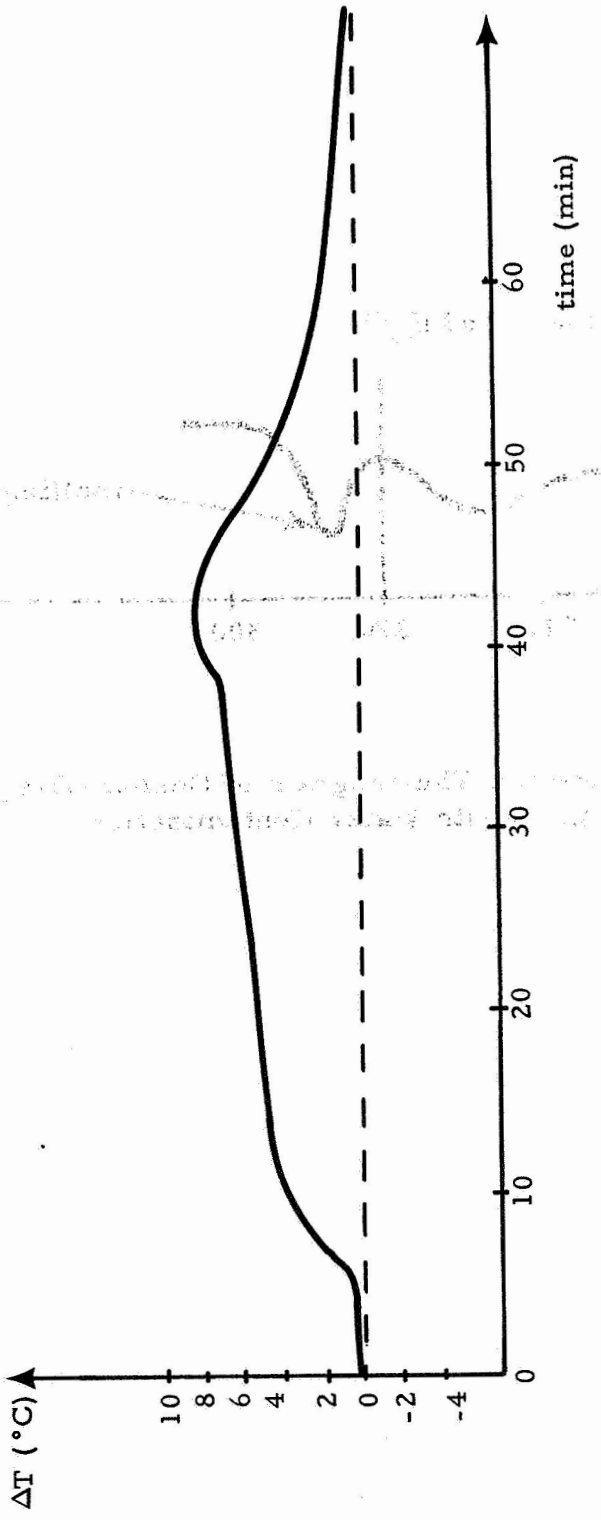

Figure II-3. Slow Oxidation of Cesium in 10% O_2 at Room Temperature as Evidenced by Differential Temperature Measurements.

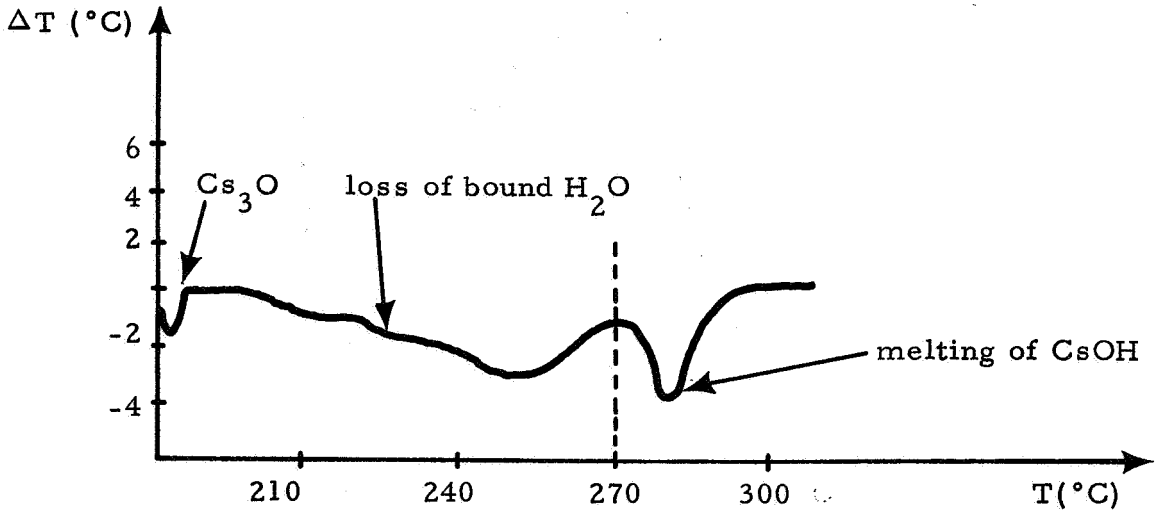

Figure II-4. Differential Thermogram of Cesium-Oxygen System (I) with Water Contamination.

A second run was made in the absence of oxygen with a new capsule of oxidized cesium. Cesium hydroxide was again present in the system, as evidenced by an endothermic peak at 270°C. A broad exothermic peak beginning at 350°C may have indicated a reaction among the cesium oxides. A small but pronounced endothermic peak was observed at 380°C, which may be related to the melting of Cs_2O_4[4] (Figure II-5).

Upon cooling, the different phases separated in the sample holder tube. The bottom and the side around the bottom of the tube were black and presumably contained, in a very thin film adherent to the wall, a mixture of suboxides (Cs_xO, where $x > 2$) with some unreacted cesium adsorbed on the tube wall. The second layer from the bottom was brown and probably contained Cs_2O and Cs_2O_3, while the top layer was white, the color reported for CsOH.

The cesium hydroxide is less dense than any of the oxides; however, the suboxides are considerably less dense than either the oxides or the hydroxide (see Table II-2). The explanation of the position of the suboxide film adhering to the wall near the bottom may be found in the high surface free energy of the suboxides and the metallic cesium as compared with the other oxides. It is remarkable that even heating the cesium sample in 10% oxygen up to 400°C for 24 hours failed to convert all the cesium to higher oxides.

In the next experiment care was taken to exclude all the water vapor from the system, and no peak was observed between 200°C and 300°C. The endothermic peak was observed at 390°C. At about 420°C a broad exothermic peak has started, possibly resulting from the reaction of cesium with the iron-constantan thermocouple; this peak was reproduced in a consecutive run where oxygen was also excluded from the system (also seen in Figure II-5).

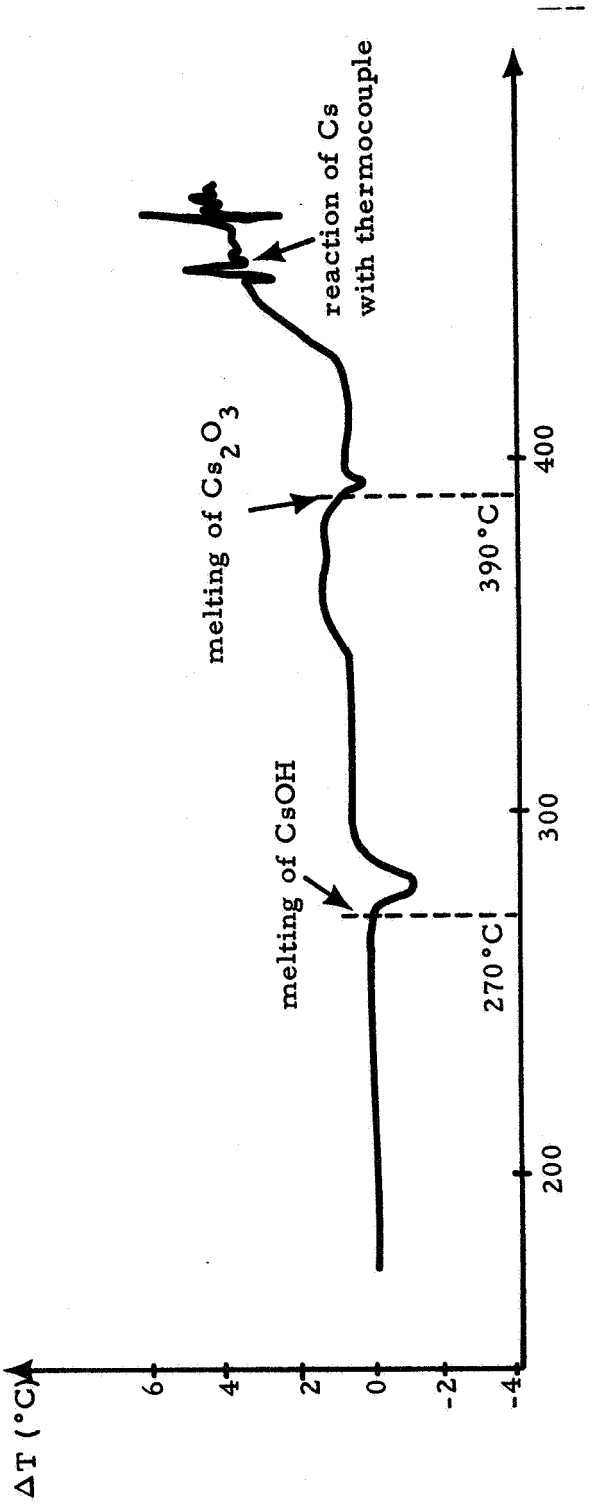

Figure II-5. Differential Thermogram of Cesium-Oxygen System (II) with Water Contamination.

TABLE II-2

OXIDES AND HYDROXIDE OF CESIUM*

Name	Chemical Symbol	Color	Density ($g \cdot gm^{-3}$)	Melting Point (°C)
cesium	Cs	silver-white	1.873	28.5
cesium hydroxide	CsOH	yellowish-white	3.675	272.3
tricesium oxide**	Cs_3O	black	2.73	~180
cesium monoxide	Cs_2O	orange-red	4.36	decomp 360-400
cesium peroxide	Cs_2O_2	yellow	4.25	400
cesium sesquioxide	Cs_2O_3	chocolate brown	4.25	400
cesium dioxide	CsO_2	yellow	3.77	600

*Data obtained from Reference 4 unless otherwise noted.

**Data obtained from Reference 3.

While cesium monoxide, Cs_2O, is expected from thermodynamic calculations, to be the dominating species under the oxidizing conditions used, it does not have a transition in the thermogram between room temperature and 400°C.

Further refinements could be made in the technique. The behavior of suboxides should be studied in some container more inert than the quartz tube, and a shielded thermocouple should be used.

C. MASS SPECTROMETER

During the second quarter the mass spectrometer system was tested with nitrogen, and a Knudsen cell designed for the analysis of cesium oxides has been built (see Figures II-6 and II-7). The Knudsen cell has been tried out in the system as a source of pure cesium and, after several minor modifications, will be ready for use with cesium oxides.

Nitrogen was used in an initial analysis of the characteristics of the system, since it is relatively inert and easily handled. Nitrogen was brought into the system through the simple gas manifold shown in Figure II-3 of the First Quarterly Report. The gas inlet was designed to produce a nitrogen beam of approximately the same density and profile as the beams to be used in cesium oxide experimentation. With the chopper (Figure II-1, First Quarterly Report) operating, the nitrogen beam could be observed easily on the scope.

With the mass spectrometer tuned to the nitrogen peak and the modulated beam "turned on," the multiplier output could easily be observed on the scope and consisted of several components:

(1) A dc component propertional to the nitrogen pressure ($\sim 10^{-7}$ torr) in the mass spectrometer chamber.

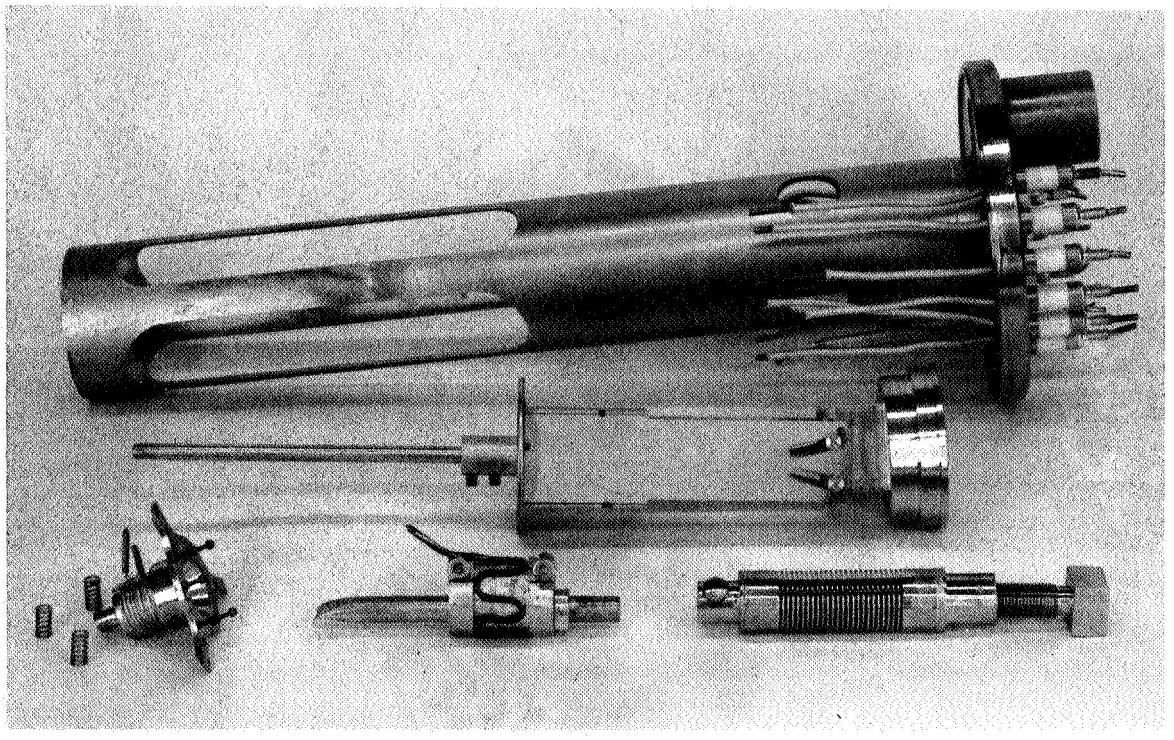

Figure II-6. Knudsen Cell Disassembled.

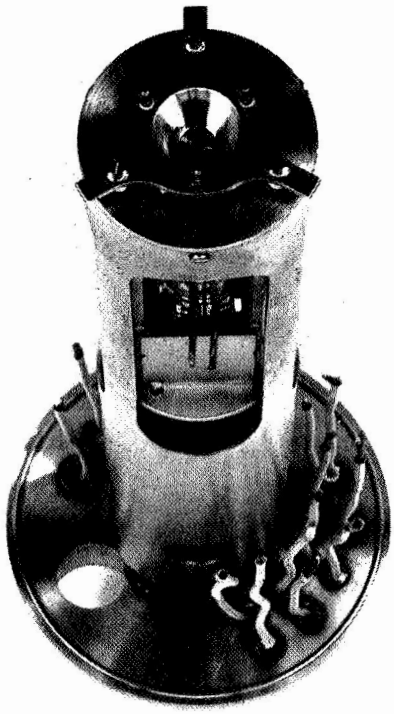

Figure II-7. Knudsen Cell Assembly.

This component is usually of no interest to us, since it represents molecules which have interacted with the walls of the system and can be eliminated with a blocking capacitor.

(2) An ac component at the modulation frequency, which could be blocked by the shutter and which was produced by particles in the direct beam. This component had a peak-to-peak amplitude of approximately 1/4 the magnitude of the dc component.

(3) A white noise (shot-type) component, which was approximately proportional to the ac signal and had a peak-to-peak amplitude of approximately 1/3 that of the modulated signal.

(4) A white noise (Johnson-type) component which is independent of beam intensity. White noise, particularly of this type, will interfere with the detection of the small signals (less than about 0.1% of the level of these nitrogen signals) which will be of interest in the cesium oxide measurements. Phase-sensitive detection will be used to circumvent this problem.

The Knudsen cell was loaded with a cesium capsule and placed into the system. After pump-down the capsule was broken, and, with the chopper in operation, the ac output of the multiplier as a function of temperature was observed. The signal as a function of temperature had the shape of the cesium vapor pressure curve, as predicted. A primary purpose for operating the system on pure cesium was to develop

procedures for handling cesium which would minimize damage to pumps and mass spectrometer. An additional problem encountered was that the molybdenum capsules designed to contain the cesium (see Fourth Monthly Report) became ductile due to heat absorbed from ion pump elements and could not be broken. Future capsules will be fabricated from vapor-deposited tungsten.

REFERENCES FOR CHAPTER II

1. Von W. Klemm und H. J. Scharf: " Auf Kenntnis der Verdampfungsvorgange bei den Alkalimetalloxiden," Z. fur anorg. und allg. Chemie, 303:236 (1960).

2. L. Brewer: " The Thermodynamic Properties of the Oxides and Their Vaporization Processes," Chem. Rev., 52:1 (1953).

3. J. E. Epperson and E. E. Stansbury," Oxidation of Cesium at Low Temperatures and Pressures," AEDC-TDR-64-195, U.S. Air Force, U. of Tennessee, Knoxville, Tenn. (1964).

4. Handbook of Chemistry and Physics, 43d Edition, p. 560, Chem. Rubber Publ. Co., Cleveland, Ohio (1961).

CHAPTER III

QUANTUM-THERMODYNAMIC DEFINITION OF ELECTRONEGATIVITY*

Elias P. Gyftopoulos and George N. Hatsopoulos

A. INTRODUCTION

Rigorous definitions are given of electronegativity of atoms, neutral or ionized, and of atomic orbitals. The definitions are consistent with the rules of the statistics of ensembles and the quantum-mechanical picture of atomic structure. The definitions have been extended to atoms in a molecule, and to atoms in a solid. The extensions, however, will be presented in future communications.

The concept of electronegativity, " the power of an atom in a molecule to attract electrons to itself" [1], has been found to be a useful tool for the correlation of a vast field of chemical knowledge and experience.[2] But in spite of the large literature on the subject, no rigorous definition of electronegativity has been suggested. The lack of definition has resulted in some confusion with respect to both the physical concept represented by electronegativity and the units of electronegativity.[3-8]

In the present communication, a free atom or a free ion is regarded as a thermodynamic system, and the electronegativity of such a system is identified with the negative of its electrochemical potential.

The electrochemical potential of a component in a phase may be evaluated by means of the theory of statistical ensembles. This theory, whether related to classical or quantum mechanics, applies to thermodynamic systems of any size.[9] Consequently, it is possible to find ensemble (thermodynamic) properties, such as the electrochemical potential, even of an atom representative of an ensemble of one-atom members. If the center of mass of each atom is fixed in space, both the one-atom members and the one-atom thermodynamic

* One of the authors (EPG) was principally supported by the National Science Foundation, Contract GK-2581.

system representative of the ensemble may be regarded as open systems having one independent component, namely electrons.

Even when all the mechanical properties of an atom, such as the energy eigenvalues and the number of electrons, assume only discrete values, the thermodynamic properties of the one-atom system representative of the ensemble, such as the energy E and the number of electrons n, assume continuous values. Each of these properties may be expressed as a continuous function of two independent thermodynamic variables.

The electrochemical potential μ is defined as the partial derivative of E with respect to n at constant entropy. This derivative must be evaluated for the ensemble passing through equilibrium states because, otherwise, it is indeterminate. This fact in turn implies that in any calculation of μ, two independent thermodynamic variables, say, n and temperature T, must be considered even if the interest is in results at zero degrees Kelvin. For example, if μ is computed as the derivative mentioned above, in order to vary n at constant entropy while the ensemble passes through equilibrium states, the temperature T must be varied. Hence, both n and T must be retained in E.

In view of these remarks, the paper is organized as follows. First, a brief review of the statistics of grand canonical ensembles is given. Second, this statistics is applied to an ensemble of one-atom members. The procedure for the calculation of the electrochemical potential is thus established. Third, electronegativity is defined as the negative of the electrochemical potential. For a neutral atom at zero degrees Kelvin, this definition yields exact results which are identical to those of Mulliken.[3] Finally, it is shown that when the

electronic structure of the atom is described by the Hartree-Fock approximation, that is when the electrons are treated as an ideal substance, an orbital electronegativity can be defined.

It should be noted that since the electrochemical potential is interpreted as the escaping tendency (the opposite of the power to attract) of a component from a thermodynamic system, it is reasonable to use the negative of this potential as a measure of electronegativity.

B. STATISTICS OF GRAND CANONICAL ENSEMBLES

Consider an ensemble of identical members, namely members which have identical possible energy eigenstates. Suppose the ensemble is in thermodynamic equilibrium, at temperature T, and that its members can exchange energy and matter with the members of a reservoir. Such an ensemble is defined as a grand canonical ensemble.[9]

For present purposes, the members of the ensemble are specified by the following conditions: (a) each member has only one independent component; (b) the energy eigenstates of each member are G_1, G_2, . . . , G_j, . . ; and (c) each energy eigenstate G_1, G_2, . . , G_j, . . is occupied by a number n_1, n_2, . . n_j, . . of particles of the component, and has an energy E_1, E_2, . . E_j, . . , respectively. Here, separate symbols for the energy and the occupation number are used for each energy eigenstate, even though more than one of these symbols may represent the same number. For example, a g-fold degenerate state is counted as g separate states.

When the laws of thermodynamics are applied to the ensemble and the reservoir,[9] it is found that the fraction x_i of members at the

energy eigenstate G_i, the probability x_i that a member is at the state G_i, is given by the relation

$$x_i = \frac{\exp[(n_i\mu - E_i)/kT]}{\sum_i \exp[(n_i\mu - E_i)/kT]}, \qquad (1)$$

where μ is the electrochemical potential of the component in the ensemble and in the reservoir, and k is Boltzmann's constant. Note that at T equals zero, x_i can be computed only as a limit.

By virtue of Eq. 1, it follows that, statistically, the average number n of particles representative of the ensemble is given by the relation

$$n = \sum_i n_i x_i$$

$$= \frac{\sum_i n_i \exp[(n_i\mu - E_i)/kT]}{\sum_i \exp[(n_i\mu - E_i)/kT]} . \qquad (2)$$

Equation 2 indicates that n is a continuous function of the continuous variables μ and T. Conversely, Eq. 2 can be solved for the continuous function $\mu(n, T)$ of the continuous variables n and T. The range of n is the same as that of the discrete values n_i.

It also follows from Eq. 1 that the average energy E of the ensemble is given by the relation

$$E = \sum_i E_i x_i . \qquad (3)$$

This energy can be thought of as a continuous function of any two of the continuous variables, n, μ, and T, and it is related to the electrochemical potential by the expression

$$\mu = \frac{\partial E}{\partial n} \quad \text{at constant entropy.} \tag{4}$$

The derivation of the last relation is given in reference 9.

C. ELECTROCHEMICAL POTENTIAL OF ATOMS AND ATOMIC IONS

Consider the special ensemble of identical, one-atom members, of atomic number Z. Suppose each member may exchange energy and only electrons with a reservoir. In thermodynamic equilibrium, this thermodynamic system constitutes a grand canonical ensemble of one component (electrons) members.

To proceed with the statistical analysis of the system, suppose first that only the ground state of the singly charged negative ion of the atomic species exists. Thus, the possible energy eigenstates of each one-atom member of the ensemble are as follows:

1. Ground states. Figure III-1 shows schematically the possible occupation numbers n_i,

$$n_i = 0, 1, 2, \ldots, Z, Z + 1, \tag{5}$$

and the corresponding energies E_i of the ground states of the neutral atom and all the positive and negative ions. It is seen from the figure that as the electron occupation number increases from zero, fully ionized atom, to Z + 1, singly charged negative ion, the energies of the corresponding ground states satisfy the relations

$$E_o > E_1 > \ldots > E_{z-1} > E_z > E_{z+1} \ . \qquad (6)$$

If the arbitrary zero energy reference level is set at the energy E_z of the neutral atom, relation 6 may be written in the form

$$I_z > I_{z-1} > \ldots > I_1 > 0 > -A_1, \qquad (7)$$

where I_i and A_i are the i-th ionization energy and electron affinity of the atom, respectively.

2. Excited states. To each occupation number n_i, smaller than or equal to Z, there corresponds an infinite number of excited states. Let the energy of each such state be denoted by E_{ij}. Each energy E_{ij} is greater than the energy E_i of the corresponding ground state.

In terms of the above energy eigenstates, the average number n of electrons representative of the ensemble is given by the relation

$$n = \frac{\sum_{i=0}^{Z+1} n_i \exp\left[(n_i\mu - E_i)/kT\right] + \sum_{i=0}^{Z} \sum_{j} n_i \exp\left[(n_i\mu - E_{ij})/kT\right]}{\sum_{i=0}^{Z+1} \exp\left[(n_i\mu - E_i)/kT\right] + \sum_{i=0}^{Z} \sum_{j} \exp\left[(n_i\mu - E_{ij})/kT\right]} \qquad (8)$$

It follows from Eq. 8 that the number of electrons of the atom, viewed as a thermodynamic system, may assume any value between 0 and Z + 1, even though the occupation numbers n_i assume only discrete values. Moreover, for given values n and T, Eq. 8 can be solved for μ. Although the general solution is numerically tedious, some general results can be readily established:

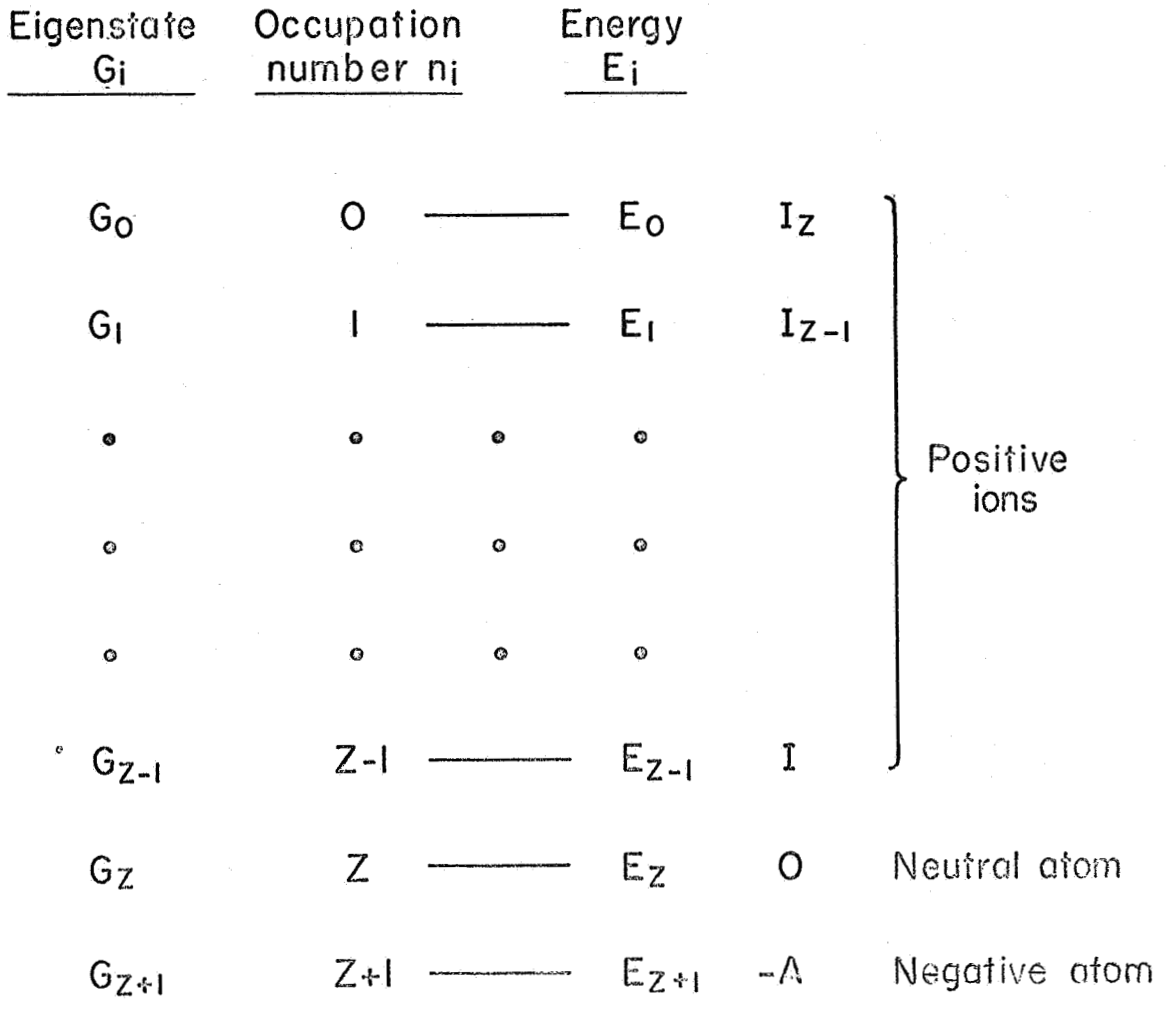

Figure III-1. Schematic of Ground States of the Neutral Atom and all the Positive and Negative Ions, of an Atom Forming only Singly Charged Negative Ions. No Degeneracies are Shown.

(i) If the ensemble is representative of either the fully ionized atom, (n equals zero) or the singly charged negative ion, (n equals Z + 1) Eq. 8 yields

$$\mu = -\omega \qquad \text{for} \qquad n = 0, \tag{9}$$

or

$$\mu = +\omega \qquad \text{for} \qquad n = Z + 1, \tag{10}$$

respectively, for all values of T. These extreme values of μ are as expected since for n equals 0 and Z + 1 the variations dn of the electron component are restricted to be only positive and negative, respectively.[10]

(ii) . For values of n in the range

$$Z < n \leq Z + 1, \tag{11}$$

μ is positive. For all other values of n, the electrochemical potential is negative. These facts can be readily verified by substitution of a non-negative value of μ in Eq. 8.

(iii) If the ensemble is representative of a neutral atom, n equals Z. For this value of n and in the limit of small temperatures, T approximately equals zero degrees Kelvin, Eq. 8 yields

$$\mu = -(I_1 + A_1)/2 + kT \ln g_{z-1} \qquad \text{for } n = Z, \text{ and } T \to 0, \tag{12}$$

where g_{z-1} is the degeneracy of the state G_{z-1}. Equation 12 is a special case of a more general result discussed below.

(iv) If the ensemble is representative of a positive ion with an integral number σ of electrons, n equals σ. For such a value of n, Eq. 8 may be written in the equivalent form,

$$\sum_{i=0}^{\sigma-1} (\sigma - n_i) \exp\left[(n_i\mu - E_i)/kT\right] + \sum_{i=0}^{\sigma-1} \sum_{j} (\sigma - n_i) \exp\left[(n_i\mu - E_{ij})/kT\right] =$$

$$= \sum_{i=\sigma+1}^{Z+1} (n_i - \sigma) \exp\left[(n_i\mu - E_i)/kT\right] + \sum_{i=\sigma+1}^{Z} \sum_{j} (n_i - \sigma) \exp\left[(n_i\mu - E_{ij})/kT\right]. \quad (13)$$

For μ negative and in the limit of small temperatures, the first sum on either side of Eq. 13 is much greater than the second. Hence, a good approximation to Eq. 13 is given by the relation

$$\sum_{i=0}^{\sigma-1} (\sigma - n_i) \exp\left[(n_i\mu - E_i)/kT\right] = \sum_{i=\sigma+1}^{Z+1} (n_i - \sigma) \exp\left[(n_i\mu - E_i)/kT\right]$$

$$\text{for } n = \sigma \text{ and } T \to 0. \quad (14)$$

For different ranges of negative values of μ, the exponents $n_i\mu - E_i$ on either side of Eq. 14 can be ordered. Given a range of values of μ suppose that the largest exponents are $\ell\mu - E_\ell$ and $r\mu - E_r$ on the left and right hand side, respectively, where

$$\ell \leq \sigma - 1 \qquad \text{and} \qquad r \geq \sigma + 1. \quad (15)$$

It follows that, in the limit of small temperatures, Eq. 14 can be approximated by the simple expression

$$g_\ell (\sigma - \ell) \exp\left[(\ell\mu - E_\ell)/kT\right] = g_r (r - \sigma) \exp\left[(r\mu - E_r)/kT\right], \quad (16)$$

where g_ℓ and g_r are the degeneracies of the states G_ℓ^* and G_r, respectively.

The last expression is satisfied for the value of μ given by the relation

$$\mu = -\left[(E_r - E_\ell) + kT \ln \frac{g_\ell(\sigma - \ell)}{g_r(r - \sigma)}\right]/(r - \ell) =$$

$$= -\left[(I_{z-r} - I_{z-\ell}) + kT \ln \frac{g_\ell(\sigma - \ell)}{g_r(r - \sigma)}\right]/(r - \ell) \quad \text{for } n = \sigma, \text{ and } T \to 0. \quad (17)$$

This value of μ is acceptable if it is within the range of values assumed for the ordering of the exponents, namely within the range which resulted in approximate Eq. 16. Otherwise, another range of μ and different values of ℓ and r must be considered.

For n equal to or smaller than Z-1, consideration of the ionization energies of atoms as specified above results in values of μ which are much smaller than that for n equals Z. For practical purposes, it is convenient (but not necessary) to assume

$$\mu = -\infty \qquad \text{for } n \leq Z - 1 \qquad \text{and all T.} \quad (18)$$

The preceding statistical analysis can be readily applied to atoms which either can form both singly and doubly charged negative ions, or cannot form negative ions. Thus, for example, for atoms which form both singly and doubly charged negative ions, n_i ranges from 0 to Z + 2, it is found that for n equals Z a possible value of μ is given by the relation

$$\mu = -(I_2 + A_2)/4 \quad \text{for } n = Z \text{ and } T = 0, \quad (19)$$

provided that

$$3 I_2 < 4 I_1 + A_2, \qquad \text{and} \qquad 4 A_1 < 3 A_2 - I_2. \tag{20}$$

D. ELECTRONEGATIVITY OF ATOMS AND ATOMIC IONS

The electronegativity of a neutral or charged atomic species is defined here as the negative of the electrochemical potential of the species viewed as a one-component member of a grand canonical ensemble. Thus, the electronegativity x(n, T) is given by the relation

$$x(n, T) = -\mu , \tag{21}$$

and is a continuous function of the continuous variables n, and T.*

Qualitatively, this definition of electronegativity is consistent with heuristic descriptions given previously. The negative of μ, the negative of the escaping tendency, represents a power to attract. A power to attract is the notion associated with electronegativity. Moreover, equality of the electrochemical potentials of a component in two different phases implies that there is no flow of this component between the two phases. In direct analogy, equality of electronegativities of two atoms implies that there is no flow of electronic charge from one atom to the other.

Quantitatively, for atoms which can form singly charged negative ions, it is seen from Eqs. 12 and 21 that the exact value of the electro-

---

* Note that when the zero energy level is set at the level of the ground state of the neutral atom, the value of the electrochemical potential equals that of the chemical potential. For this energy reference level, the electronegativity equals the negative of the chemical potential.

Note also that x can be expressed as a continuous function of another pair of continuous thermodynamic variables, say, entropy and temperature.

negativity x(Z, 0) of the neutral atom is given by the relation

$$x(Z, 0) = (I_1 + A_1)/2. \qquad (22)$$

This value is identical to the approximate value recommended by Mulliken.[3] Also, the exact value of the electronegativity given by the negative of Eq. 10 was suggested by Mulliken[3] without reference to the restrictions represented by relations 20.

E. ORBITAL ELECTRONEGATIVITY

The discussion in Section C and the definition of electronegativity in Section D are presented without any reference to the procedure employed for the determination of the possible energy eigenstates of the members of the ensemble. Consideration of the approximate methods used for the calculation of the energy eigenvalues leads to the concept of orbital electronegativity.

To see this point clearly, consider a Z-electron atom. The quantum-mechanical analysis of the electronic structure of this atom is very difficult. The difficulty is avoided if the electrons are treated as an ideal substance, that is the Z-electron Hamiltonian operator is reduced to an approximate sum of Z separable, one-electron Hamiltonian operators. The reduction can be made by means of different approximate methods. One of these is the Hartree-Fock method.

The Hartree-Fock, one-electron operator defines an energy eigenvalue problem. Each eigenfunction of this operator, one-electron orbital, can accommodate at most two electrons with opposite spins. When the orbital is occupied by an electron with a given spin, it is called

a spin-orbital. The negative of each eigenvalue is interpreted as an ionization energy. This interpretation is based on the assumption that the extraction of the electron from the corresponding orbital does not perturb the eigenstates of the other electrons, and it is known as Koopmans' theorem.[11] Finally, the energy of a given state of the atom is given approximately by the sum of the energies of the occupied spin-orbitals.

This way of thinking about the atom has the following implications for an atom which forms only singly charged negative ions.

(a) The energies I_1 and A_1 of the atom may be thought of as the ionization energy and the electron affinity of a valence orbital, respectively.

(b) Variations of the charge of the atom, regarded as a thermodynamic system, in the range

$$Z - 1 \leq n \leq Z + 1 \tag{23}$$

may be thought of as occurring because of continuous variations of the charge in the valence orbital.

(c) For values of n in the range represented by relations 23, the energy E(n, T) (Eq. 3) is a function of the charge in the valence orbital only. This statement is justified by Koopmans' theorem.

(d) Suppose that the average charge in the valence orbital is represented by q, so that

$$q = +e \text{ for } n = Z-1,\ q = 0 \text{ for } n = Z, \text{ and } q = -e \text{ for } n = Z+1,$$

where e is the electronic charge. At zero temperature, the energy and electrochemical potential of the atom may be thought of as the

energy $\epsilon_o(q)$ and the electrochemical potential $\mu_o(q)$ per unit charge of the valence orbital, respectively. From the results of Section 4, it is readily verified that for

$$\begin{aligned} &q = e,\ \epsilon_o(q) \equiv I_1,\ \mu_o(q) \equiv -\infty, \\ &q = 0:\ \epsilon_o(q) \equiv 0,\ \mu_o(q) \equiv -(I_1 + A_1)/2e, \\ &q = -e:\ \epsilon_o(q) \equiv -A_1\ \mu_o(q) \equiv +\infty. \end{aligned} \tag{24}$$

These values suggest that $\epsilon_o(q)$ and $\mu_o(q)$ may be represented by the approximate continuous functions given by the relations

$$\epsilon_o(q) = \frac{I_1 + A_1}{2e}\, q + \frac{I_1 - A_1}{2}\left[1 - \left(1 - \frac{q^2}{e^2}\right)^{1/2}\right], \tag{25}$$

and

$$\mu_o(q) = -\frac{d\epsilon_o(q)}{dq} =$$

$$= -\frac{I_1 + A_1}{2e} - \frac{I_1 - A_1}{2}\,\frac{(q/e)}{\left[1 - (q/e)^2\right]^{1/2}}. \tag{26}$$

(e) It follows that, at zero temperature, the electronegativity of the atom may be thought of as an orbital electronegativity $x_o(q)$ given by the approximate relation

$$x_o(q) = \frac{d\epsilon_o}{dq} = \frac{I_1 + A_1}{2e} + \frac{I_1 - A_1}{2}\,\frac{(q/e)}{\left[1 - (q/e)^2\right]^{1/2}}. \tag{26}$$

(f) Similar statements can be made about other types of atoms.

Expressions somewhat analogous to those represented by Eqs. 24 and 26 have been introduced heuristically by other authors.[12] These authors expressed doubts about the validity of the assumption that both $\epsilon_o(q)$ and $x_o(q)$ are continuous functions of the continuous variable q. In view of the present work, it is seen that orbital electronegativity is obtained from basic quantum-thermodynamic arguments and that, indeed, $\epsilon_o(q)$ and $x_o(q)$ are continuous functions of the continuous thermodynamic variable q.

The preceding approach to the definition of electronegativity has been extended to atoms in molecules and solids. The results will be presented in future communications.

REFERENCES FOR CHAPTER III

1. L. Pauling, The Nature of the Chemical Bond, Cornell University Press, Ithaca, New York, 3rd edition, pp. 3-27, (1960).

2. C.A. Coulson, Proc. Roy. Soc. (London), A207, 63, (1951).

3. R.S. Mulliken, J. Chem. Phys. 2, 782, (1934); 3, 573, (1935).

4. J.G. Malone, J. Chem. Phys. 1, 197, (1933).

5. W.E. Gordy, and W.J. Orville Thomas, J. Chem. Phys., 24, 439, (1956).

6. H.O. Pritchard, and H.A. Skinner, Chem. Rev. 55, 745, (1955).

7. J. Hinze, and H.H. Jaffé, J. Am. Chem. Soc. 84, 540, (1962).

8. R. Ferreiva, J. Phys. Chem. 68, 2240, (1964).

9. G.N. Hatsopoulos and J.H. Keenan, "Principles of General Thermodynamics," J. Wiley, New York, Ch. 48, (1965).

10. J.W. Gibbs, "The Scientific Papers of J. Willard Gibbs," Vol. 1, Dover Publications, New York, pp. 135-138, (1961).

11. J.C. Slater, "Theory of Molecules and Solids," Vol. 1, McGraw Hill, New York, p. 96, (1963).

12. J. Hinze, M.A. Whitehead, and H.H. Jaffé, J. Am. Chem. Soc. 85, 148, (1963).

CHAPTER IV

PARAMETRIC DATA

D. Lieb, F. Rufeh, L. van Someren, C. Wang

A. SINGLE-CRYSTAL TUNGSTEN CONVERTER

A variable-spacing, guard-ring converter with a single-crystal tungsten emitter and a molybdenum collector was constructed during the first quarter. Experimental data from this converter, covering a wide range of emitter temperatures and interelectrode spacings, were presented in the First Quarterly Report.[1] During the second quarter these data were analyzed, and additional data were obtained.

1. Work-Function and Variable-Spacing Data

The emitter work function was determined from saturation currents obtained under ion-rich conditions. Typical raw data is shown in Figure IV-1, and the reduced data is plotted as a function of T_E/T_R in Figure IV-2. The work function of polycrystalline tungsten is also shown for reference in this figure. The cesiated work function of single-crystalline 110 tungsten is about 0.2 volt less than that of polycrystalline tungsten.

Variable-spacing families of volt-ampere characteristics were also obtained. Figure IV-3 shows the effect of interelectrode spacing on both the extinguished and ignited modes. The products of cesium pressures and interelectrode spacings used form a consistent set with the data reported in the First Quarterly Report.[1]

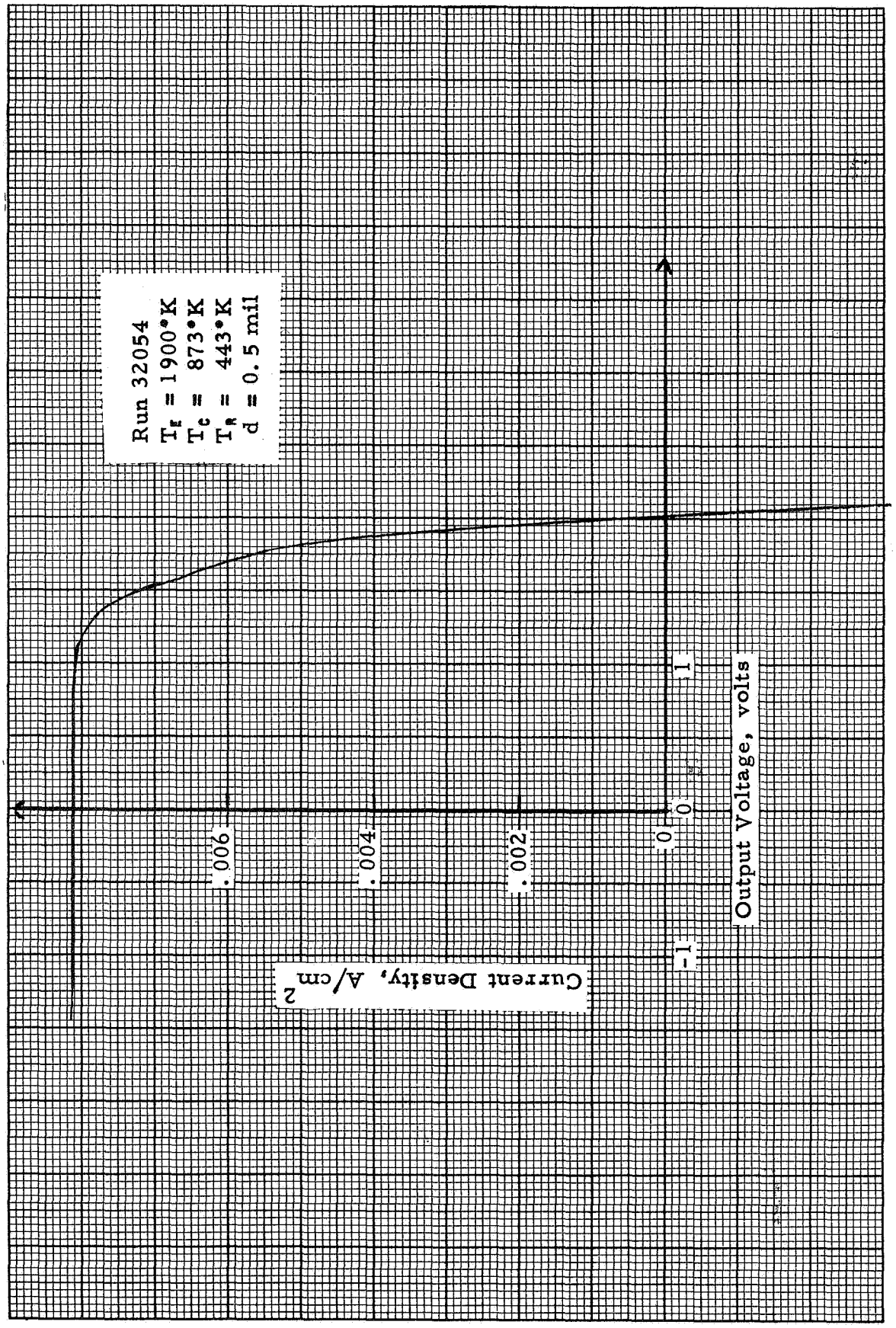
Run 32054
T_E = 1900°K
T_C = 873°K
T_R = 443°K
d = 0.5 mil
Current Density, A/cm^2
.006
.004
.002
0
-1
-0.5
0
0.5
1
Output Voltage, volts

Figure IV-1

68-TR-4-7

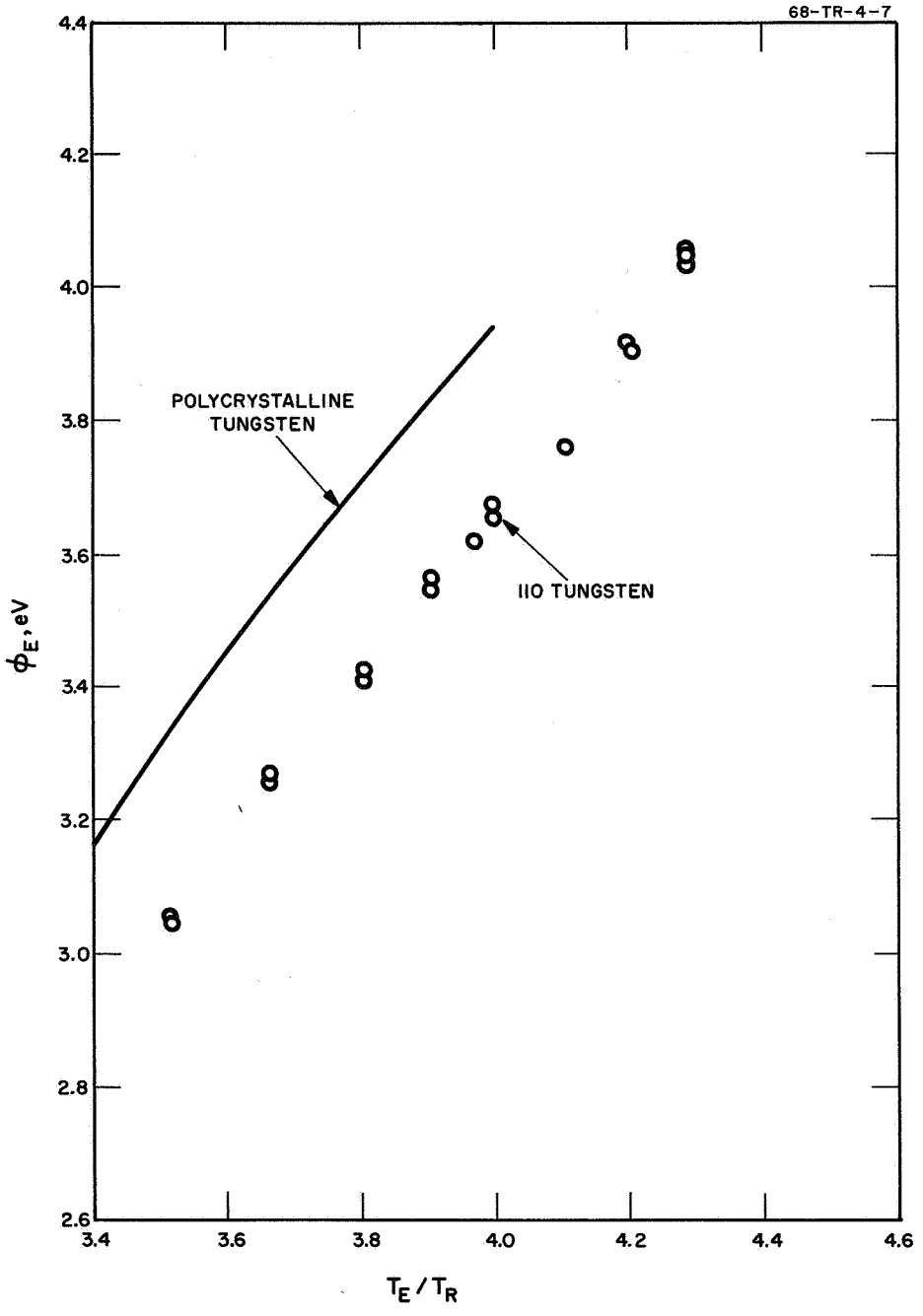

Figure IV-2

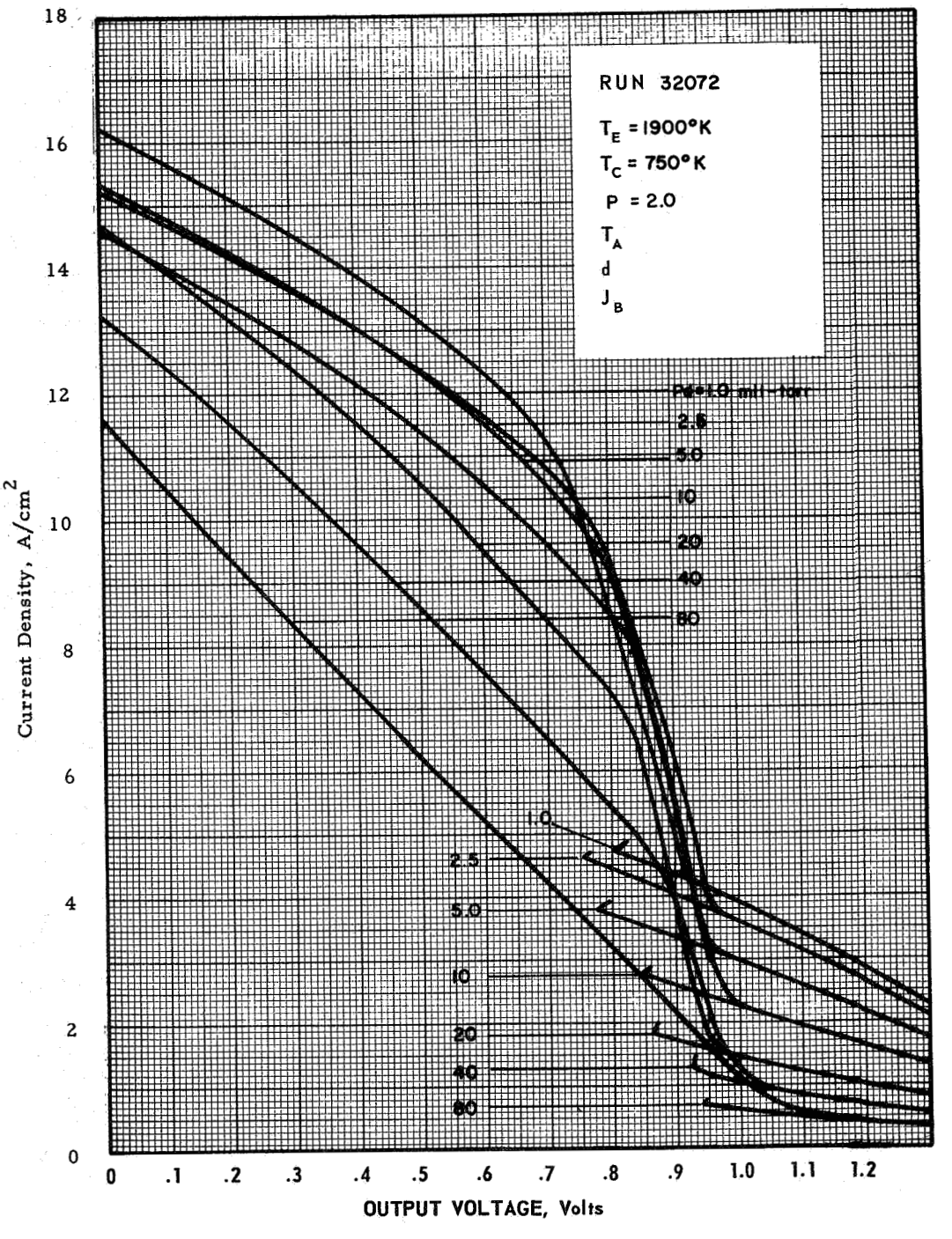
RUN 32072
T_E = 1900°K
T_C = 750°K
P = 2.0
T_A
d
J_B
Cs*1.0 milli-torr
2.5
5.0
10
20
40
80
1.0
2.5
5.0
10
20
40
80
Current Density, A/cm^2
OUTPUT VOLTAGE, Volts
0
2
4
6
8
10
12
14
16
18
0
.1
.2
.3
.4
.5
.6
.7
.8
.9
1.0
1.1
1.2

Figure IV-3

2. Internal Voltage Drop Correlation

One of the important correlations which has been found in the past[2] is the dependence of the internal voltage drop, V_d, on the product of cesium pressure and interelectrode spacing, Pd. This was, however, only a first-order correlation, and deviations were observed which could not be accounted for by the experimental errors. It is suspected that there are other dependencies which contribute to the deviations from the V_d correlation.

One of the goals of the present program is an investigation of the possible dependence of V_d on parameters such as cesium pressure, P, and ion richness, β, at constant values of Pd.

a. Procedure

A series of cesium families of volt-ampere characteristics covering a wide range of interelectrode spacings and emitter temperatures was presented in the First Quarterly Report.[1] The cesium pressures and the interelectrode spacings were selected in such a manner as to provide a large number of volt-ampere characteristics for various combinations of P, Pd and β. These cesium families were used to study the possible dependencies of the internal voltage drop in the above parameters.

Each cesium family forms an envelope which is tangent to the individual J-V curves (Figure IV-4). For the purpose of this analysis, V_d was defined as the difference in voltage between the point of tangency and the Boltzmann curve. The point of tangency was chosen, since it is readily identified and since maximum power and maximum efficiency occur near that point. In establishing the Boltzmann curves,

the collector work function was assumed to be 1.6 eV. This assumption is reasonable since the data was obtained at optimum collector temperature.

b. Results

Figure IV-5 shows the voltage drop, at a pressure of 1.42 torr, as a function of Pd for three values of T_E/T_R. The constant values of T_E/T_R represent approximately constant values of ion richness, β. Similar data for other cesium pressures are shown in Figures IV-6 through IV-8. These data suggest that the internal voltage drop is decreasing function of ion richness.

Figure IV-9 shows V_d, at $T_E/T_R = 3.4$, as a function of Pd for several cesium pressures. Similar data for other values of T_E/T_R are shown in Figures IV-10 through IV-12. It appears that the voltage drop also depends on P at constant values of Pd and T_E/T_R.

c. Limitations of the Present Correlation and Conclusions

The experimental data suggest that the internal voltage drop is a function of Pd, P and β. These results, however, are tentative, and further investigation is required to obtain more definite conclusions. As described previously, the Boltzmann curve was established using a collector work function of 1.6 eV. An alternative technique is to determine the collector work function for each J-V curve from T_C/T_R plots. The latter technique will be applied in the near future. Furthermore, the results presented in this section were obtained from one converter. It is suspected that the internal voltage drop is also a function of electrode surface parameters such as bare work function and surface uniformity. These effects will be studied when additional data becomes available.

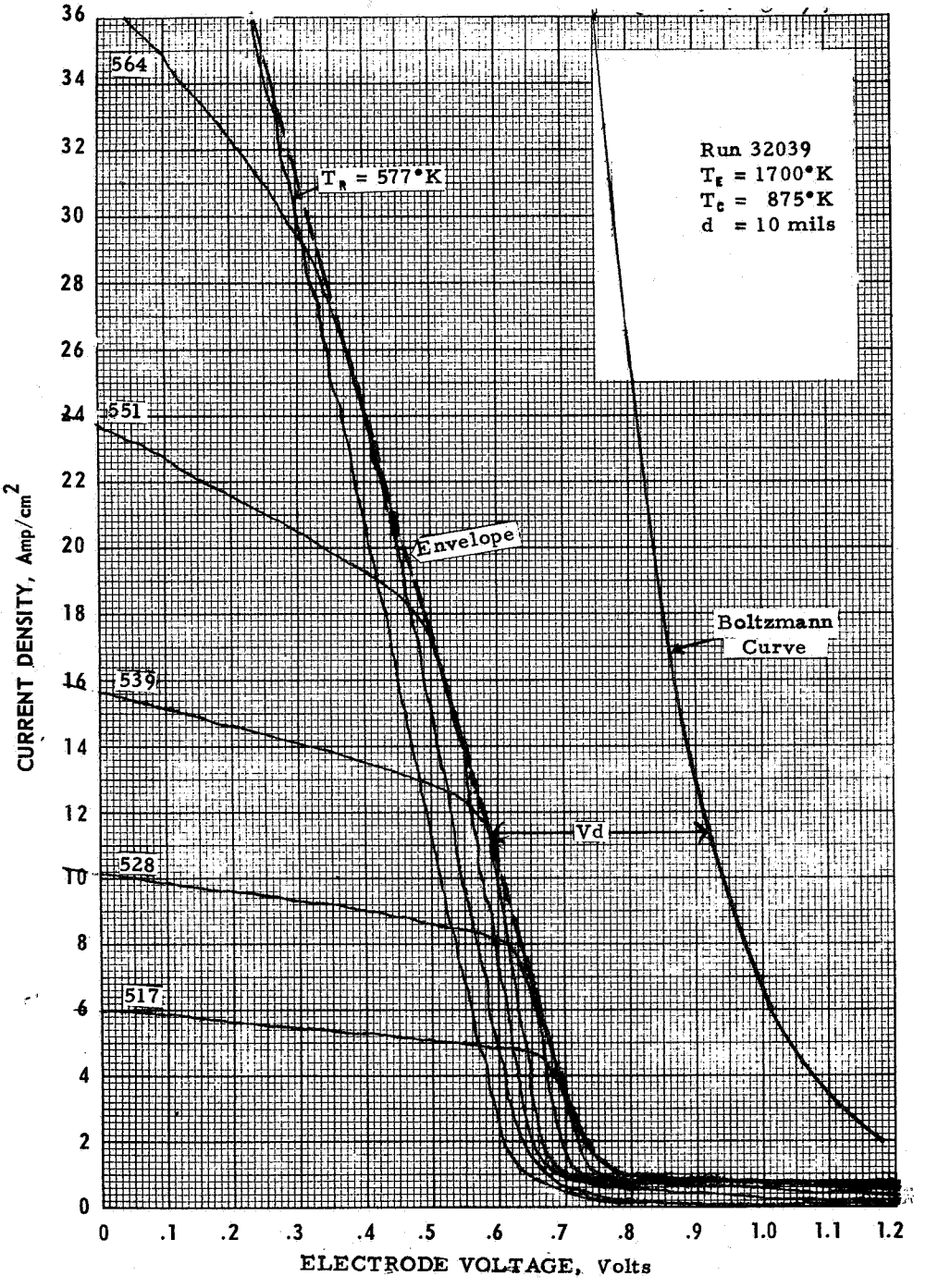
Run 32039
T_E = 1700°K
T_c = 875°K
d = 10 mils
564
551
539
528
517
T_R = 577°K
Envelope
Boltzmann Curve
Vd
CURRENT DENSITY, Amp/cm^2
ELECTRODE VOLTAGE, Volts
0
2
4
6
8
10
12
14
16
18
20
22
24
26
28
30
32
34
36
0
.1
.2
.3
.4
.5
.6
.7
.8
.9
1.0
1.1
1.2

Figure IV-4

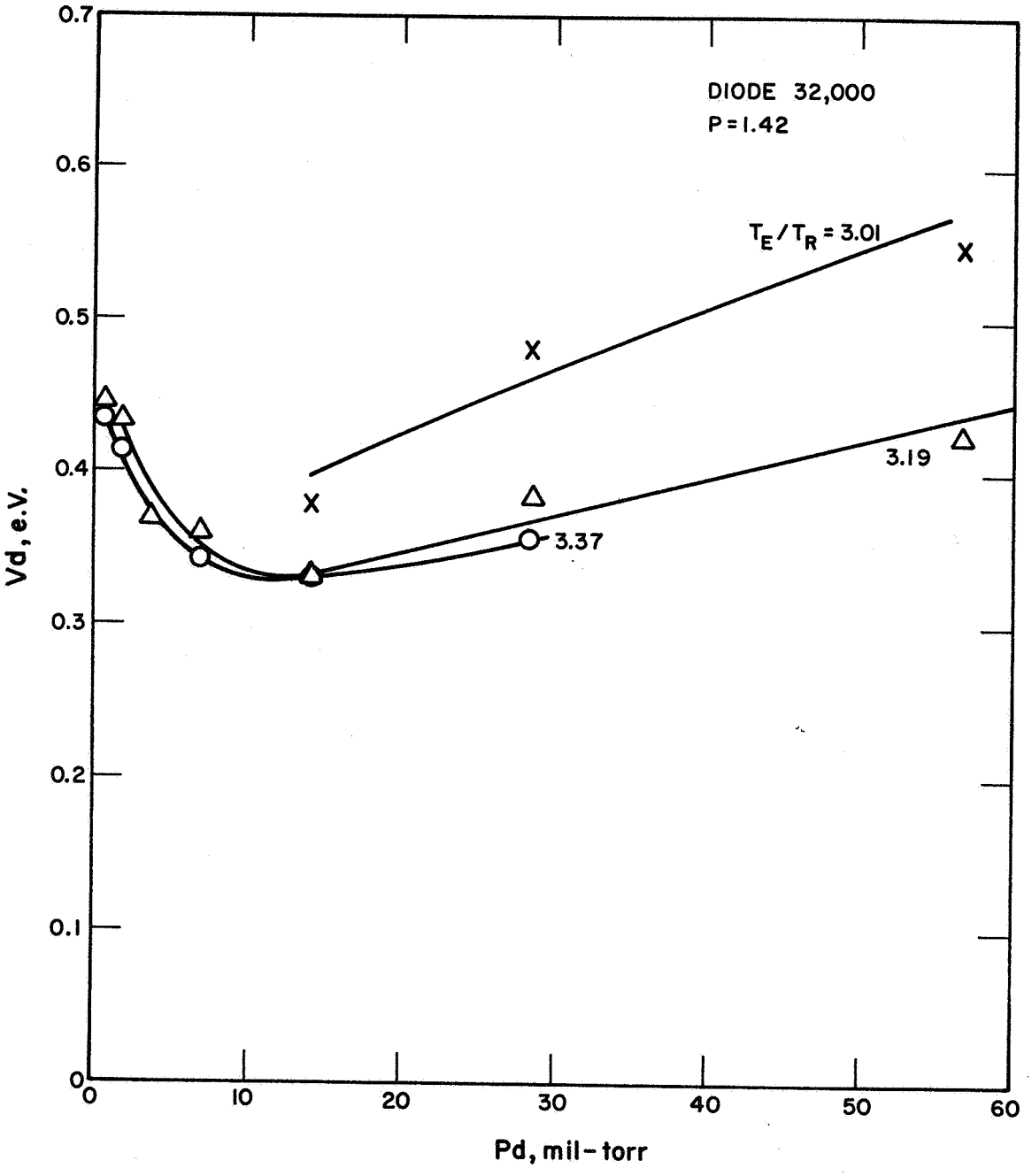
DIODE 32,000
P=1.42
T_E/T_R = 3.01
3.19
3.37
Vd, e.V.
Pd, mil-torr
0.7
0.6
0.5
0.4
0.3
0.2
0.1
0
0
10
20
30
40
50
60

Figure IV-5

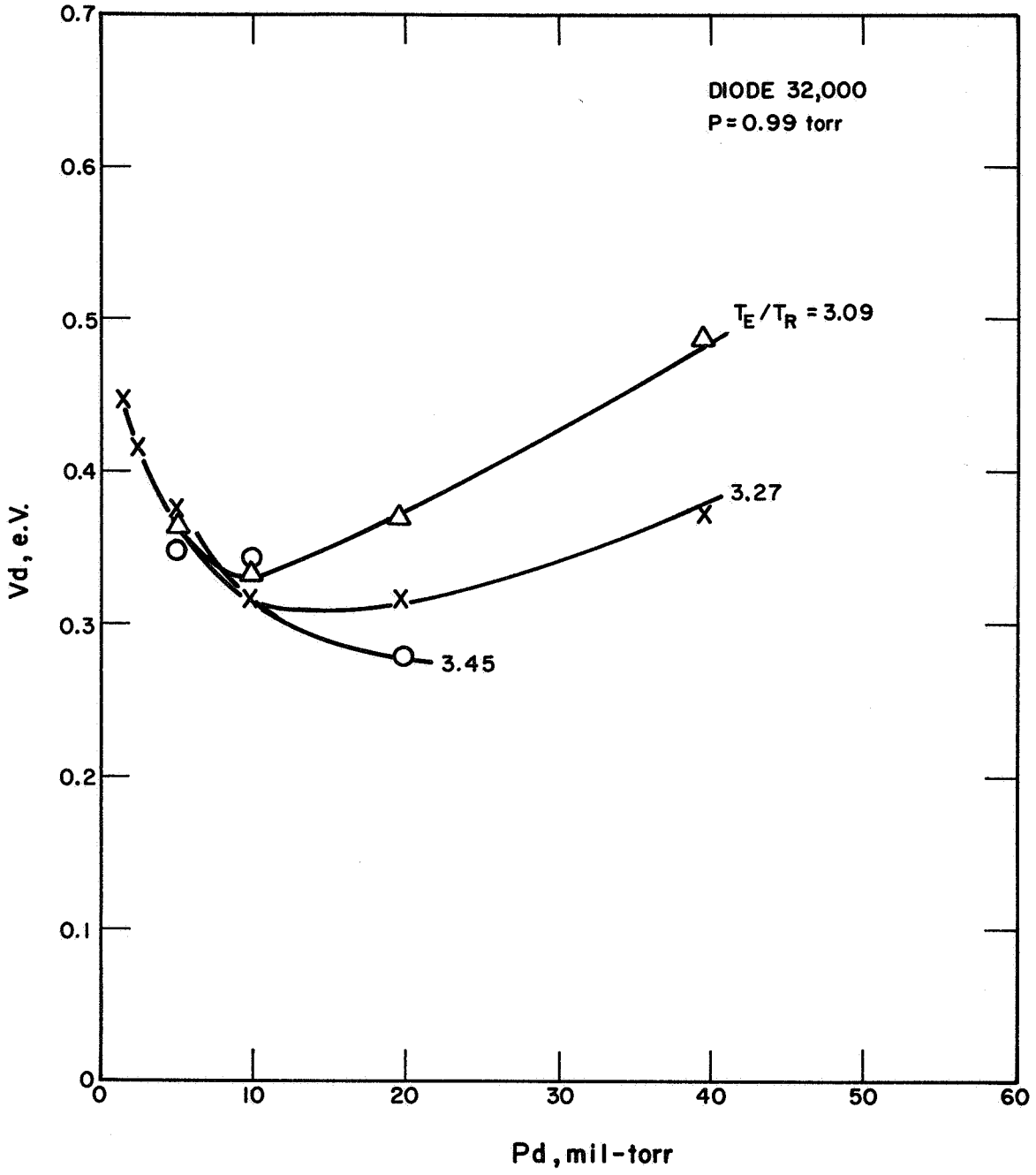
DIODE 32,000
P = 0.99 torr
T_E/T_R = 3.09
3.27
3.45
Vd, e.V.
Pd, mil-torr
0.7
0.6
0.5
0.4
0.3
0.2
0.1
0
0
10
20
30
40
50
60

Figure IV-6

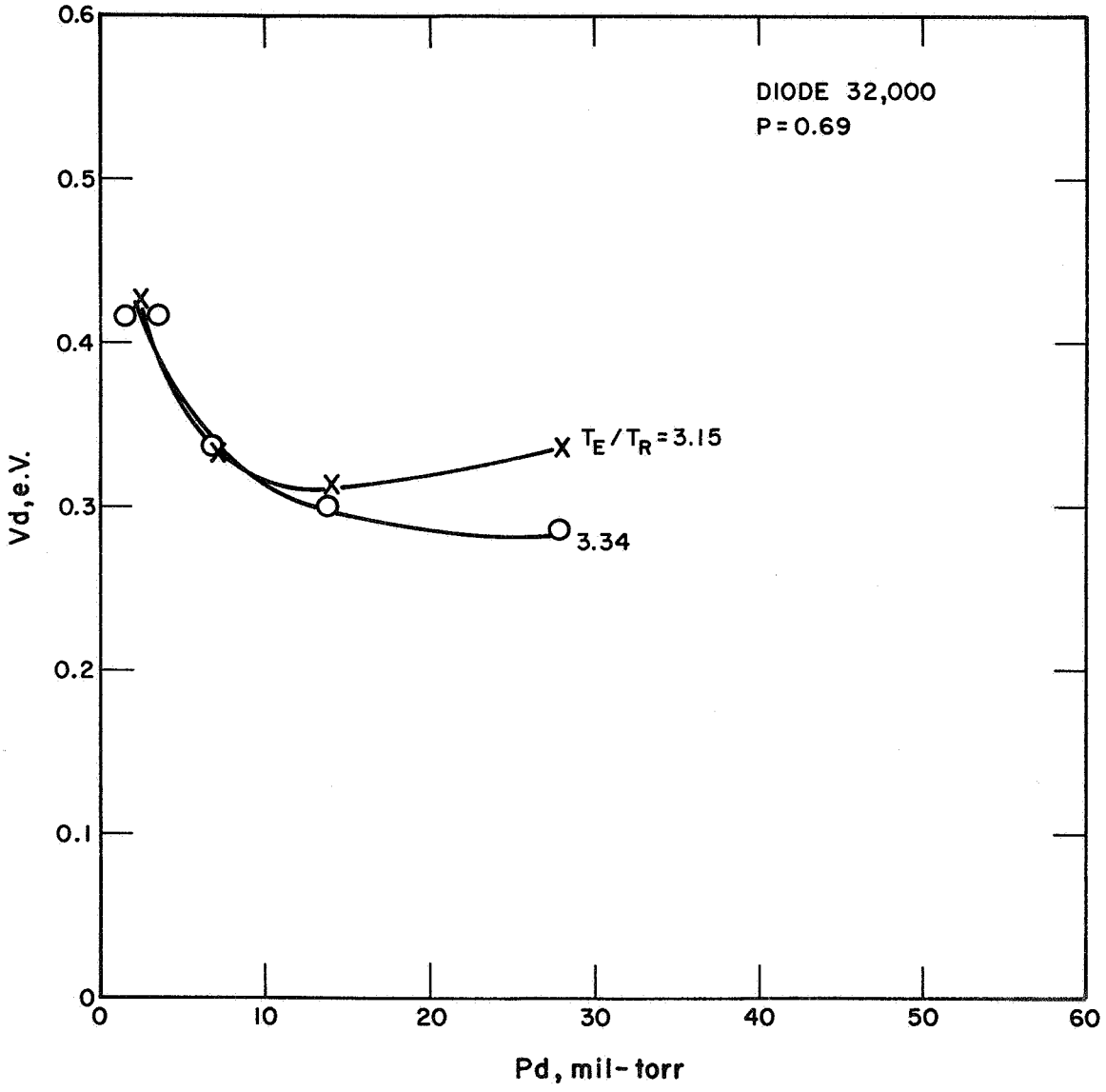
DIODE 32,000
P = 0.69
$T_E / T_R = 3.15$
3.34
Vd, e.V.
Pd, mil-torr
0.6
0.5
0.4
0.3
0.2
0.1
0
0
10
20
30
40
50
60

Figure IV-7

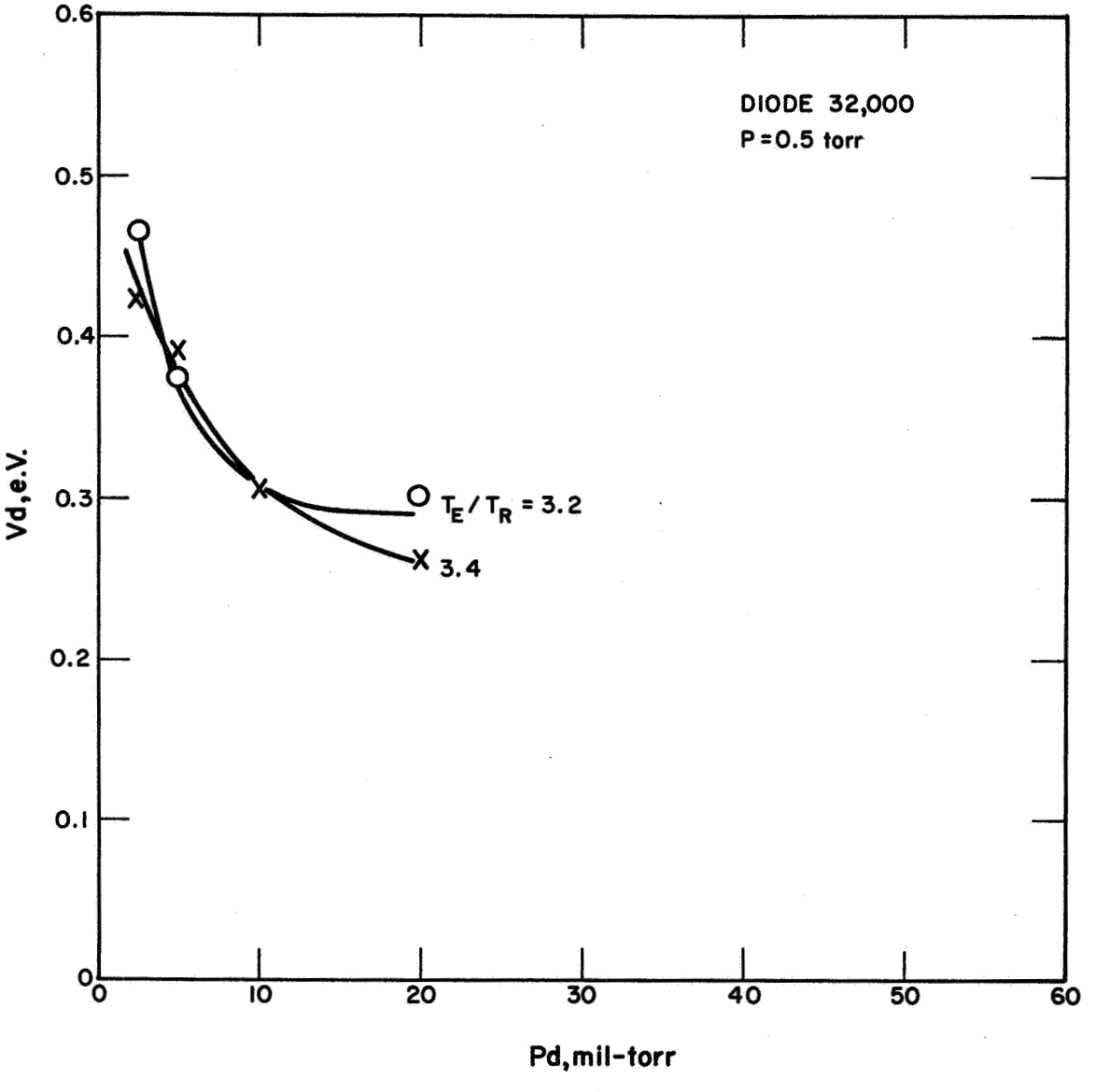
DIODE 32,000
P=0.5 torr
T_E / T_R = 3.2
3.4
Vd, e.V.
Pd, mil-torr
0.6
0.5
0.4
0.3
0.2
0.1
0
0
10
20
30
40
50
60

Figure IV-8

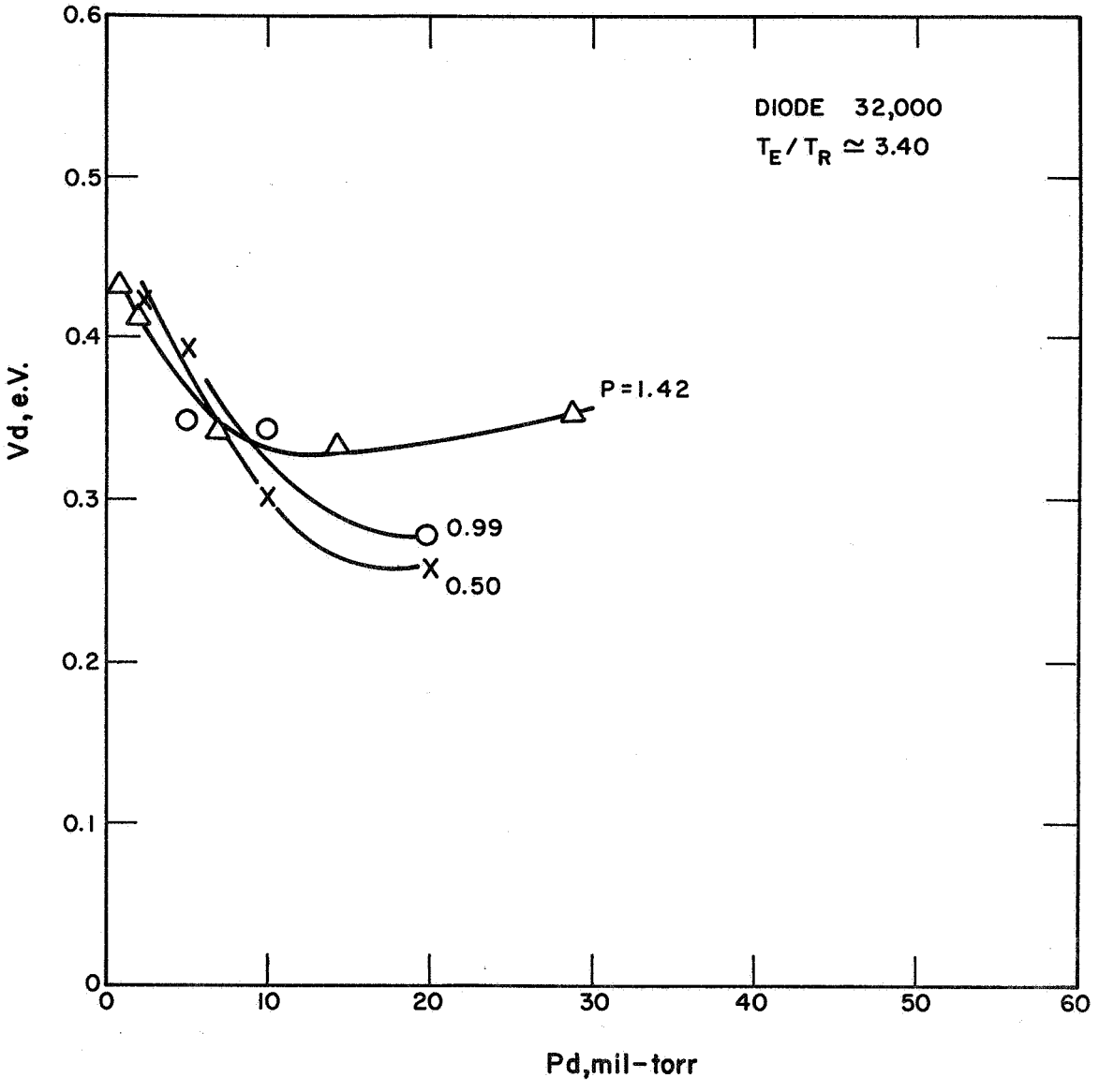
DIODE 32,000
$T_E / T_R \simeq 3.40$
P=1.42
0.99
0.50
Vd, e.V.
Pd, mil-torr
0.6
0.5
0.4
0.3
0.2
0.1
0
0
10
20
30
40
50
60

Figure IV-9

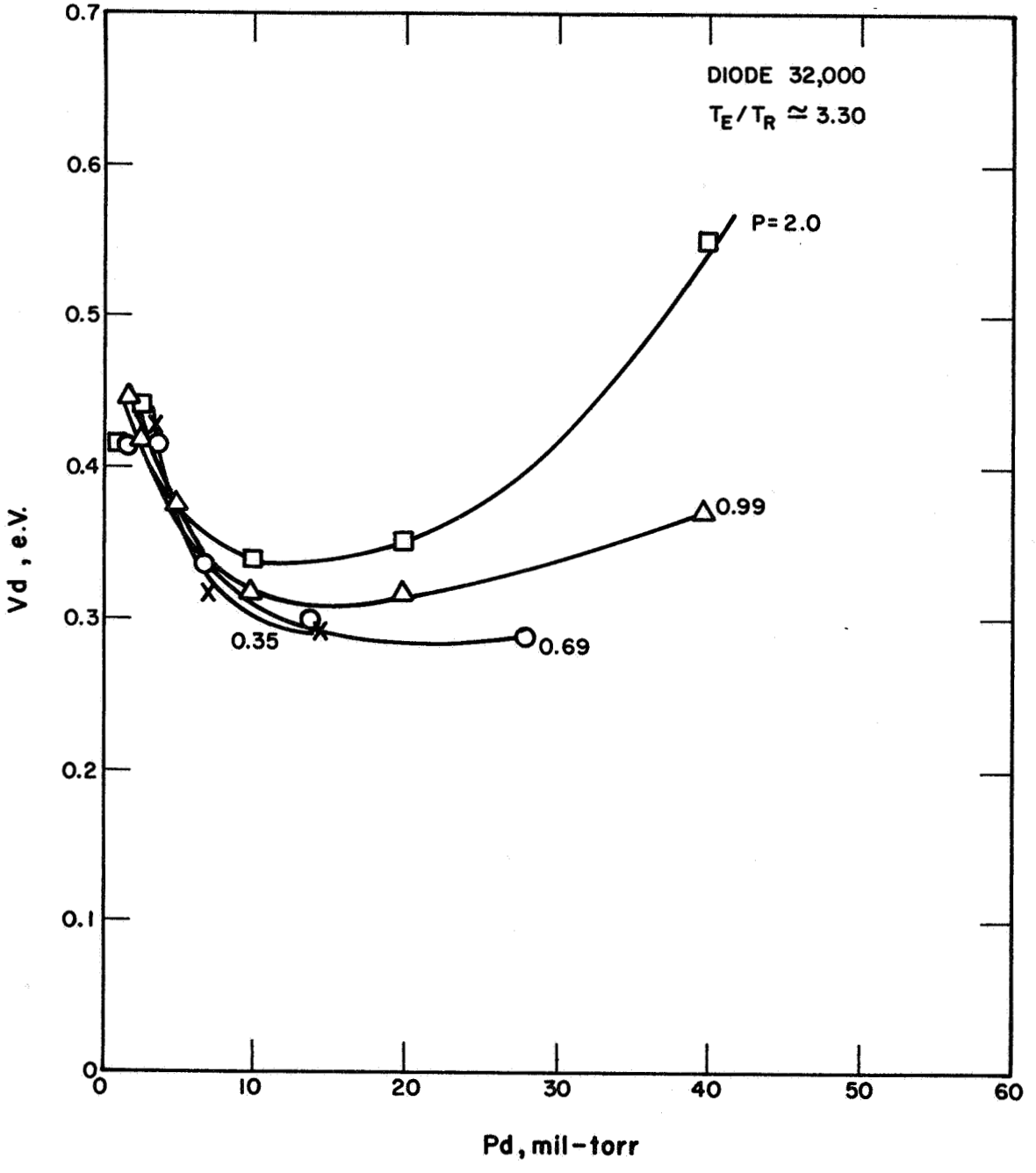
DIODE 32,000
$T_E / T_R \simeq 3.30$
P=2.0
0.99
0.35
0.69
Vd, e.V.
Pd, mil-torr
0.7
0.6
0.5
0.4
0.3
0.2
0.1
0
0
10
20
30
40
50
60

Figure IV-10

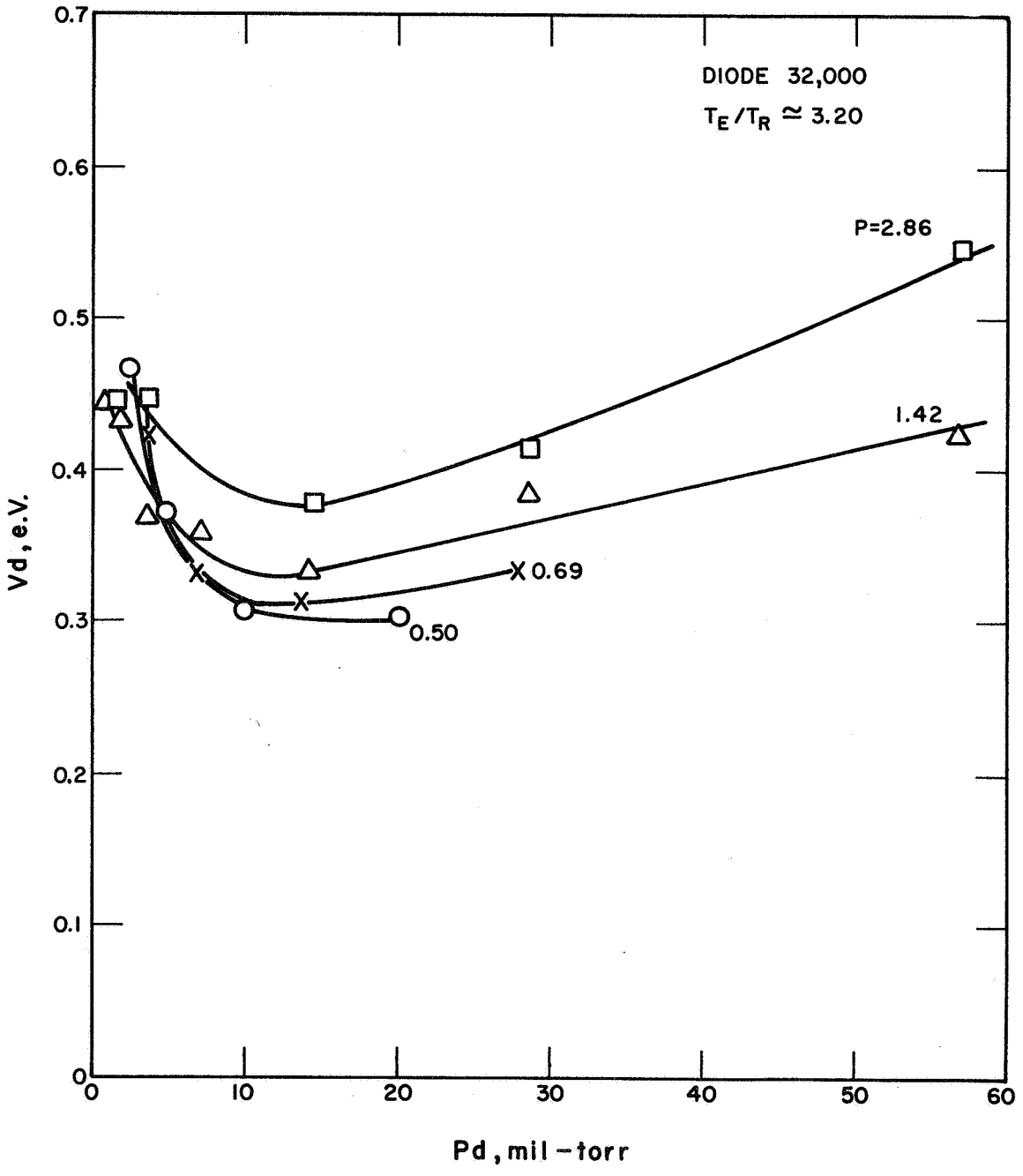
DIODE 32,000
$T_E/T_R \simeq 3.20$
P=2.86
1.42
0.69
0.50
Vd, e.V.
Pd, mil-torr
0.7
0.6
0.5
0.4
0.3
0.2
0.1
0
0
10
20
30
40
50
60

Figure IV-11

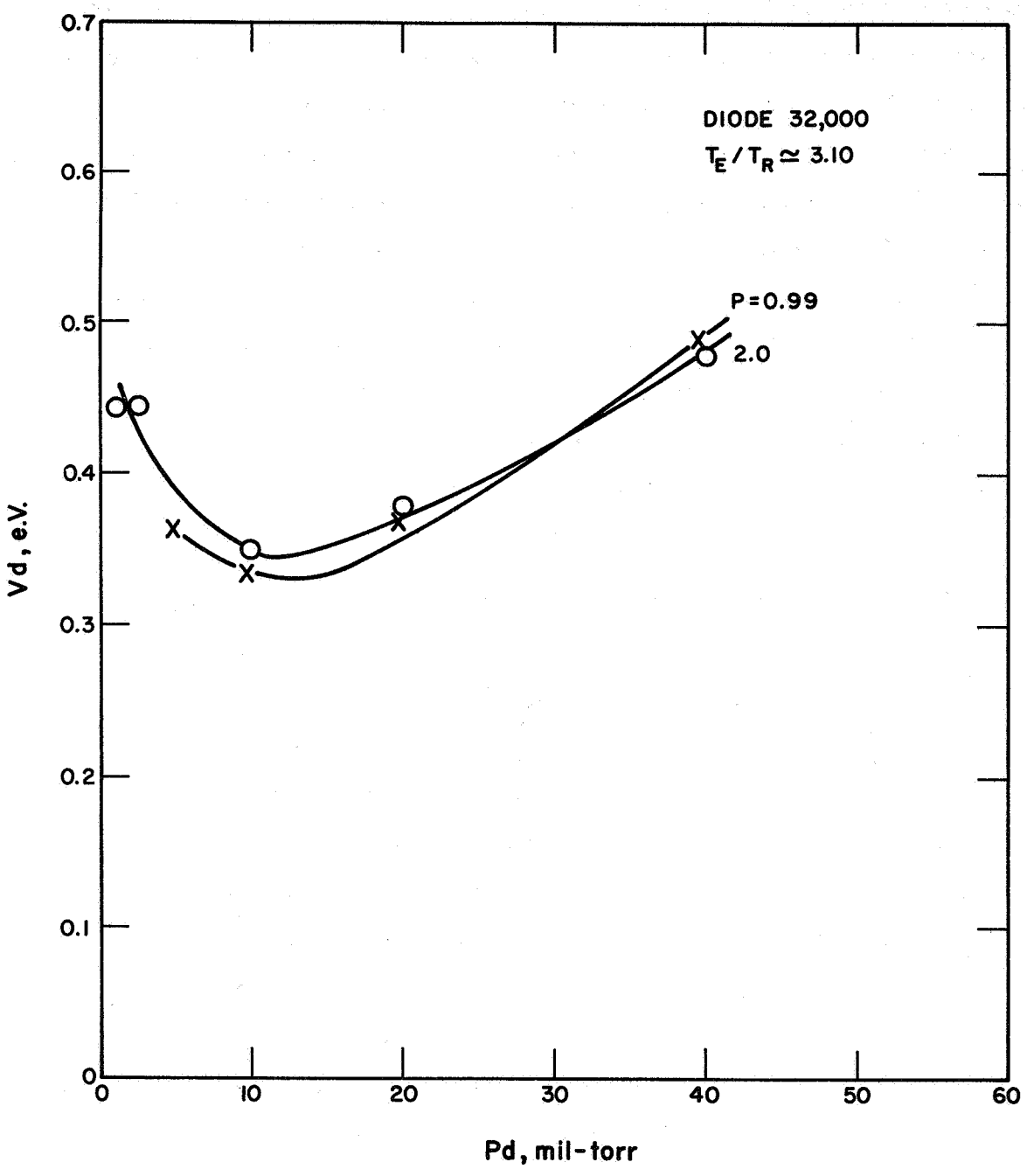
DIODE 32,000
$T_E / T_R \simeq 3.10$
P=0.99
2.0
Vd, e.V.
Pd, mil-torr
0.7
0.6
0.5
0.4
0.3
0.2
0.1
0
0
10
20
30
40
50
60

Figure IV-12

B. FLUORIDE VAPOR-DEPOSITED TUNGSTEN CONVERTER

A variable-spacing converter with a fluoride vapor-deposited tungsten emitter and a molybdenum collector was constructed in order to obtain data for comparison with in-pile test converters. The emitter was made from an ingot of approximately 0.2-inch-thick material obtained from San Fernando Laboratories, and described in more detail in the First Quarterly Report on this program. The top of the deposit, which was to be the emitting surface, was ground flat. The emitter was then fired at vacuum ($< 5 \times 10^{-5}$ torr) for 20 minutes at 1900°C. After treatment the surface showed grinding marks and slight grain boundary grooving. Examination of the emitter surface by x-ray diffraction showed considerable recrystallization of the random layer induced by grinding (Figure IV-13). The degree of orientation is still less than in the as-deposited material.

The converter has been cesiated and is ready for testing.

C. VACUUM WORK FUNCTION TEST CELL

Recent results of bare emitter work function measurements in cylindrical converters have shown a correlation between high bare work function values and good converter performance. Meaningful measurements of bare emitter work function require an ultra-high-vacuum environment and high emitter temperatures to minimize the influence of oxygen contamination. These conditions are more severe than are usually encountered in cesium converters. The design of a test device which satisfies the above requirements has been completed; this cell will be used to study the correlation between work function and performance.

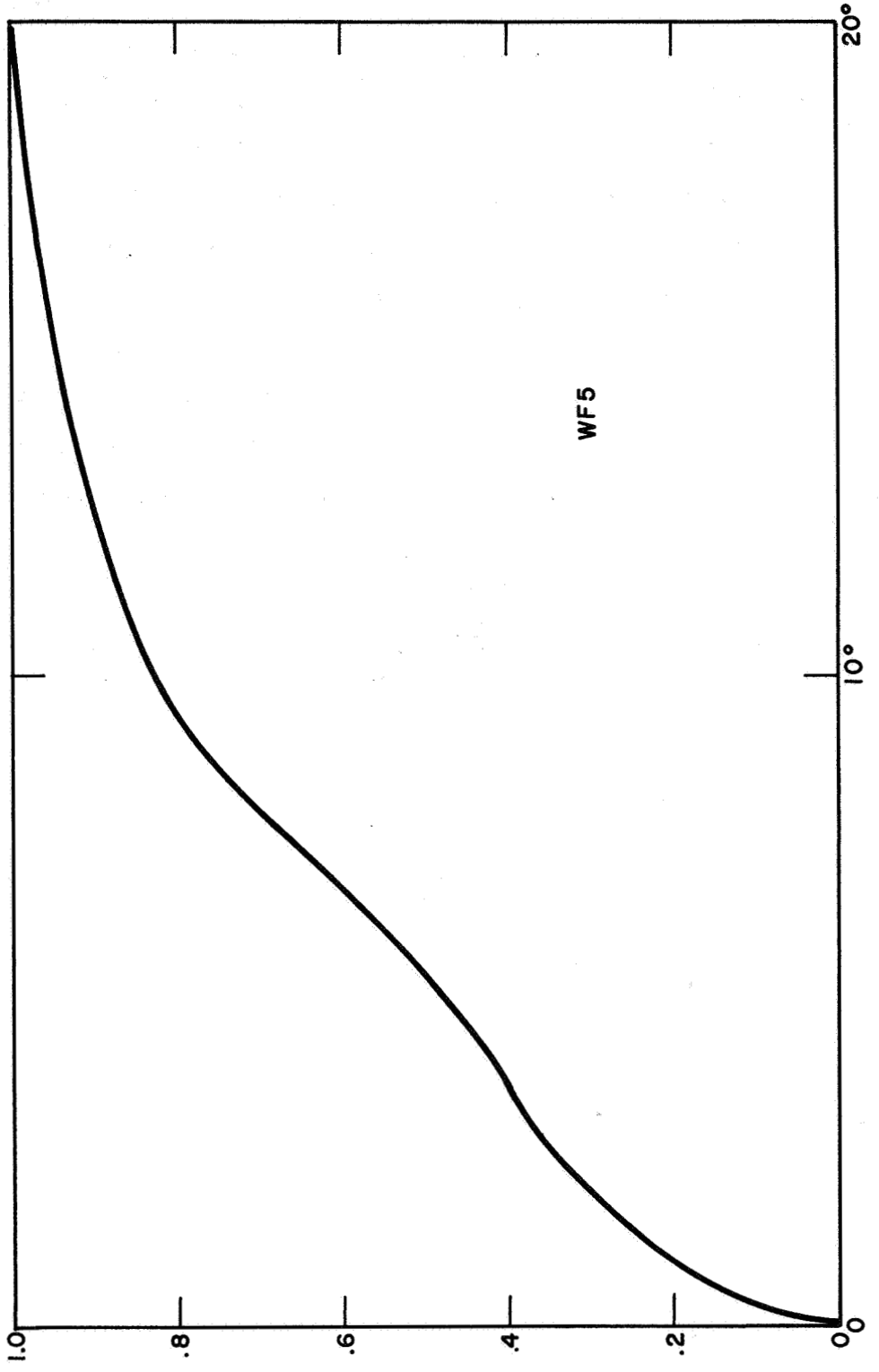

Figure IV-13

The schematic of the test cell is shown in Figure IV-14. It uses a guarded, water-cooled collector and getter ion pumping. The emitter is heated by electron bombardment and operates at a maximum temperature of about 2300°K. Emitter temperature is measured by an optical pyrometer from the window on the side or on the bottom of the system. Since the emitter is held in place by gravity, no welds or brazes are required for its mounting, and different-sized slugs can be accommodated by changing the supporting disk. Before the bottom window is sealed in place, the spacing can be set to the desired value with an adjusting screw. Copper gaskets on the various flanges and a roughing valve with a metal seal are used to avoid oxygen contamination. The collector is heated for outgassing by radiation from the emitter.

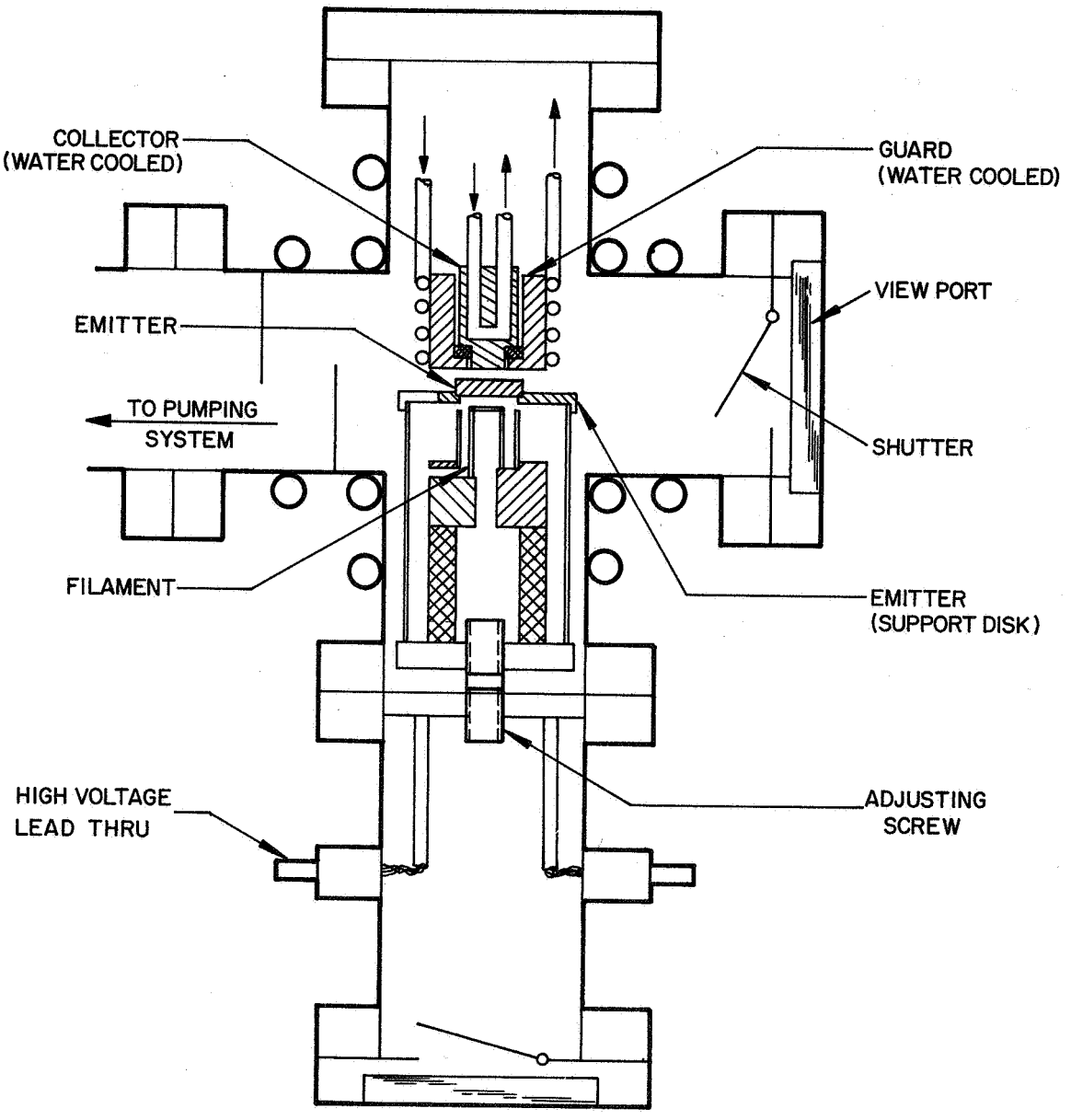
COLLECTOR
(WATER COOLED)
GUARD
(WATER COOLED)
VIEW PORT
EMITTER
TO PUMPING
SYSTEM
SHUTTER
FILAMENT
EMITTER
(SUPPORT DISK)
HIGH VOLTAGE
LEAD THRU
ADJUSTING
SCREW

Figure IV-14

REFERENCES FOR CHAPTER IV

1. Chapter IV, First Quarterly Progress Report, Applied Thermionic Research (Contract 952184), December 1967 to March 1968. Thermo Electron Report No. TE4092/3-123-68.

2. Second Annual Technical Summary Report for the Thermionic Emitter Materials Research Program, Contract NONR-3563(00), July 1962 through September 1963. Thermo Electron Report No. TE27-64.

CHAPTER V

STUDIES OF VAPOR-DEPOSITED TUNGSTEN EMITTER MATERIALS

L. van Someren

During this quarter work has continued on the structural changes in vapor-deposited tungsten following heat treatment. Both fluoride and chloride materials have been studied by optical microscopy and by x-ray diffraction. The materials studied are from the same lots as those reported during the first quarter on this program.

A. FLUORIDE MATERIAL

Sample WF3 was subjected to heat treatment for 6 hours at 2400°C, and the resulting grain structure showed a change at the discontinuity near the center of the deposit (Figure V-1). The grains at the bottom of the deposit showed grain growth and smoothing of grain boundaries, as expected, but in certain regions of the specimen, including that shown in Figure V-1, the upper part of the deposit showed massive grain growth to give grains with dimensions of a few millimeters. These grains terminated at the discontinuity near the middle of the deposit.

Sample WF4 was subjected to successive heat treatments, each at 1800°C, for 6 hours, 6 + 24 = 30 hours, and 6 + 24 + 70 = 100 hours. Cross sections at each stage are shown in Figures V-2, -3, and -4. While the first two figures cover the same area, it was not possible to identify this area after 100 hours, owing to changes in the grain structure. The difference in contrast between grains in the latter figures is due to differences in etching techniques.

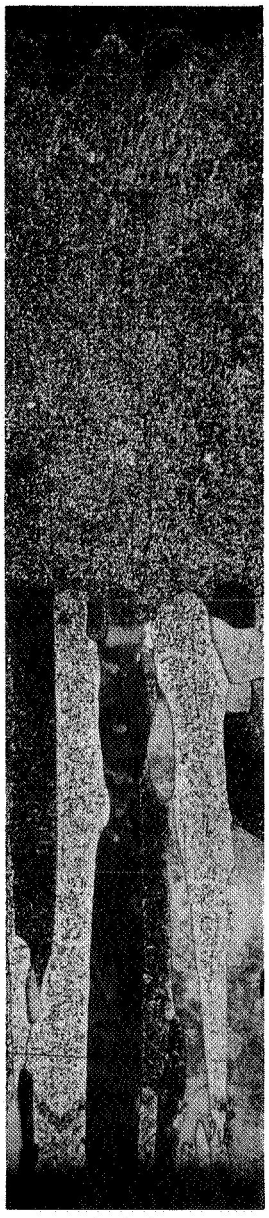

Figure V-1. Cross-section of sample WF3B' after 6 hours at 2400°C.

68-R-6-59

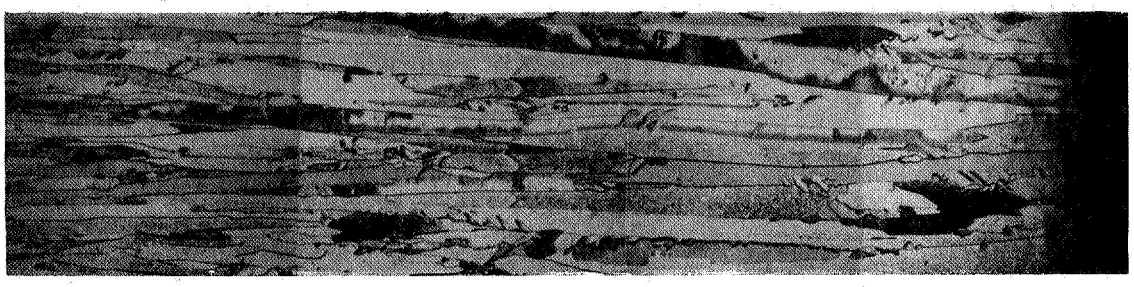

Figure V-2. Cross section of sample WF4B' after 6 hours at 1800°C.

68-R-6-60

Figure V-3. Cross section of sample WF4C' after 30 hours at 1800°C.

68-R-6-61

Figure V-4. Cross section of sample WF4D' after 100 hours at 1800°C.

Grain growth has continued to occur during the heat treatment, accompanied by the elimination of some of the angularities along the grain boundaries. Comparison of Figure V-4 with Figure V-1 indicates that further grain growth does occur in specimens exposed to higher temperatures. It is not clear whether the configuration in Figure V-4 would change further at 1800°C or would require a higher temperature to initiate further changes.

B. CHLORIDE MATERIAL

Specimen WC1 was subjected to heat treatment for 6 hours at 1900°C. Photomicrographs of cross sections before and after are shown in Figures V-5 and V-6. Massive grain growth has occurred, particularly in the outer layers which originally contained the longest columnar grains.

Specimen WC6 was subjected to heat treatment for 1 hour at 2000°C, and the resulting cross section is shown in Figure V-7. Grain growth has occurred to an extent similar to that in WC1B, Figure V-6. These observations confirm those reported previously that the grain structure of chloride material is far less stable to heat treatment than is that of fluoride material.

It was mentioned in the first quarterly report that in certain cases material evaporated from chloride specimens during their heat treatment. In an effort to determine the origin and nature of the material, a sample was collected and examined by emission spectroscopy. It was found to be tungsten, containing small traces (< 0.01%) of Cr, Fe, Ni, Si and Mb. Since metallic tungsten would not have evaporated at the temperatures in question, the manufacturer was consulted, who suggested that unreduced

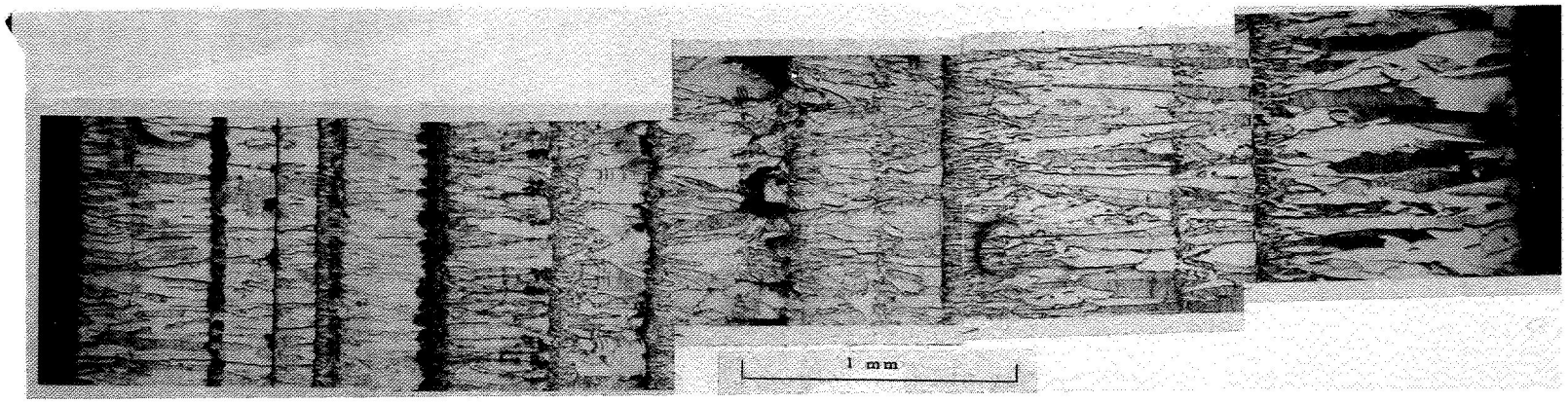

Figure V-5. Cross section of sample WC1A as received. The scale for this figure applies to all other cross sections of this type.

68-R-6-63

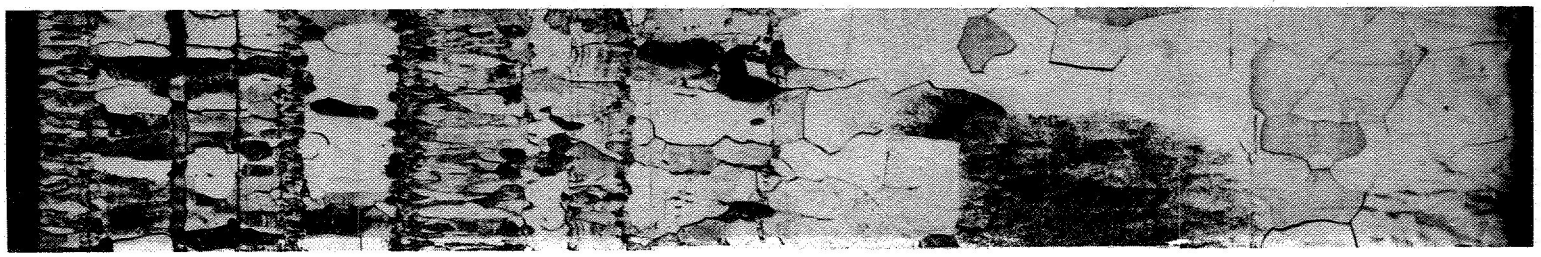

Figure V-6. Cross section of sample WC1B' after 6 hours at 1900°C.

Figure V-7. Cross section of sample WC6B' after 1 hour at 2000°C.

tungsten chlorides might have been present in the material, which could also account for the striated appearance of certain regions of the material, such as that in Figure V-16 of the first quarterly report. The chlorides are much more volatile than tungsten metal. They are also soluble in water, and so a preliminary attempt was made to dissolve some, by boiling crushed fragments of chloride tungsten in distilled water. This did not extract enough chloride to give a visible precipitate when silver nitrate solution was added, but the manufacturer's hypothesis cannot be ruled out.

Additional emission-spectroscopic examinations were carried out on the as-received fluoride and chloride material, and they gave the following results for metallic impurities in parts per million:

	10 to 100	1 to 10	0.3 to 3	0.1 to 1 ppm
Chloride	Si	Cu	Fe Ni Mo	Mg
Fluoride	—	Si Mo	Cu	Mg

Thus the chloride material was probably better than 99.995% pure W, and the fluoride better than 99.998% pure, excluding gases and interstitials.

C. MORPHOLOGY OF DEPOSITS

In the course of examination of fluoride material it became possible to show that the bounding surface of the deposit was composed largely of pyramids bounded by {111} planes. This is consistent with the unsupported observation of Holman and Huegel.[1] Slightly below the surface of the deposit in some areas there lay a zone of material with a high etch-pit density. This is visible in Figure V-7 of the first quarterly report, and is shown in more detail in Figure V-8 here.

[1] W. R. Holman and F. J. Huegel, CVD Tungsten Process Development in "CVD of Refractory Metals . . . ," Report on ANS-AIME Conference at Gatlinburg, Tenn., Sept. 1967, Ed. A. C. Schaffhauser, page 144.

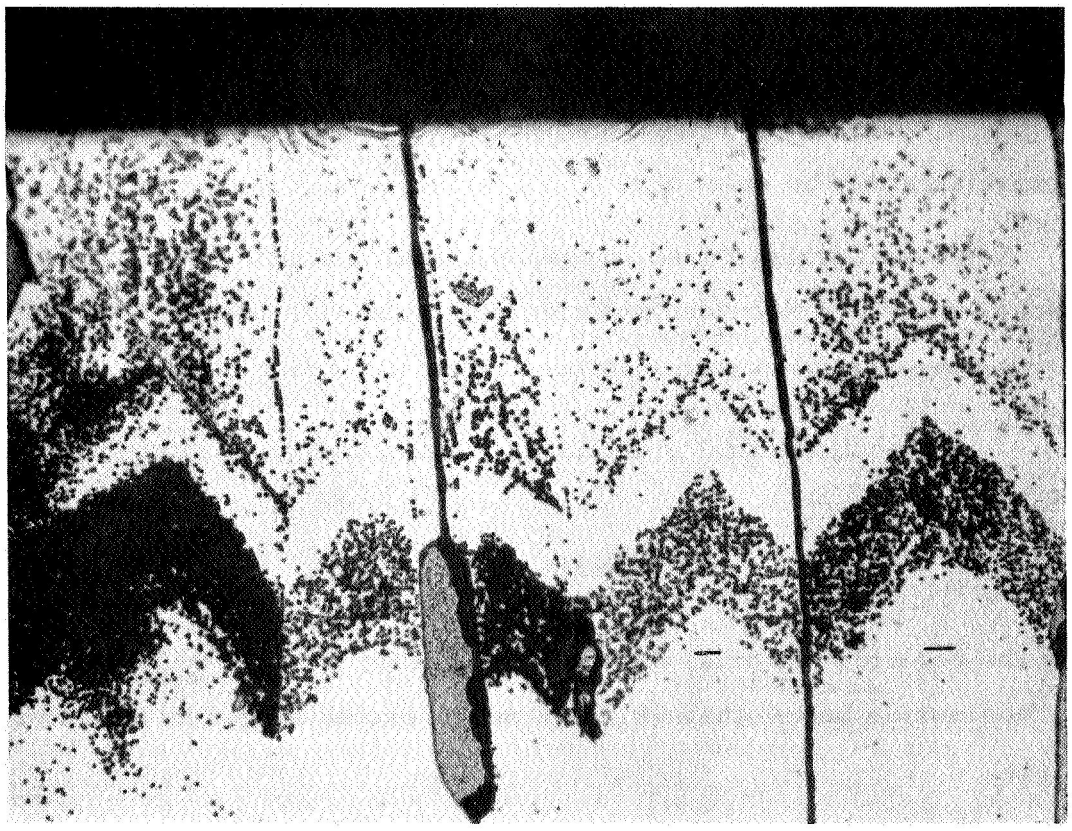

Figure V-8. Cross section of sample WF2C' showing high-etch-pit-density zone near ground surface. (225X)

This zone presumably represents a small perturbation in the growth conditions, similar to that found near the mid-plane of the deposit and discussed above. We shall make the assumption that the zone was everywhere parallel to the surface of the deposit at the time when the zone was growing. The view in Figure V-8 is perpendicular to the plane of the deposit and shows a slice through the four-sided pyramids which terminate each columnar grain. These pyramids might be composed of four {110} planes or four {111} planes.

A section in the plane of the deposit (on another specimen from the same ingot) is shown in Figure V-9. Here the photograph plane passes through the high-etch-pit-density (or "dark-etching") zone at about the position indicated by dark marks on Figure V-8, and reveals that the dark-etching zone is square and surrounds a clear zone in each grain. This is consistent with the ideas that each grain terminates in a four-sided pyramid and that the dark-etching zone was parallel to the pyramidal growth surface.

It can be shown that a pyramid of {110} planes will have a square trace on a (100) plane with edges lying in ⟨100⟩ directions, while a pyramid of {111} planes will have a square trace on a (100) plane with edges lying in ⟨110⟩ directions. Therefore, the choice between these two types of pyramidal plane resolves to determining the crystallographic direction which the edges of the dark-etching zone make in each grain. Examination of many grains, of which that in Figure V-10 is typical, shows that the dark-etching zone edges always lie at a 45° angle to the edges of individual etch pits. An independent experiment using a (100)-oriented single crystal revealed that the etch pits have edges

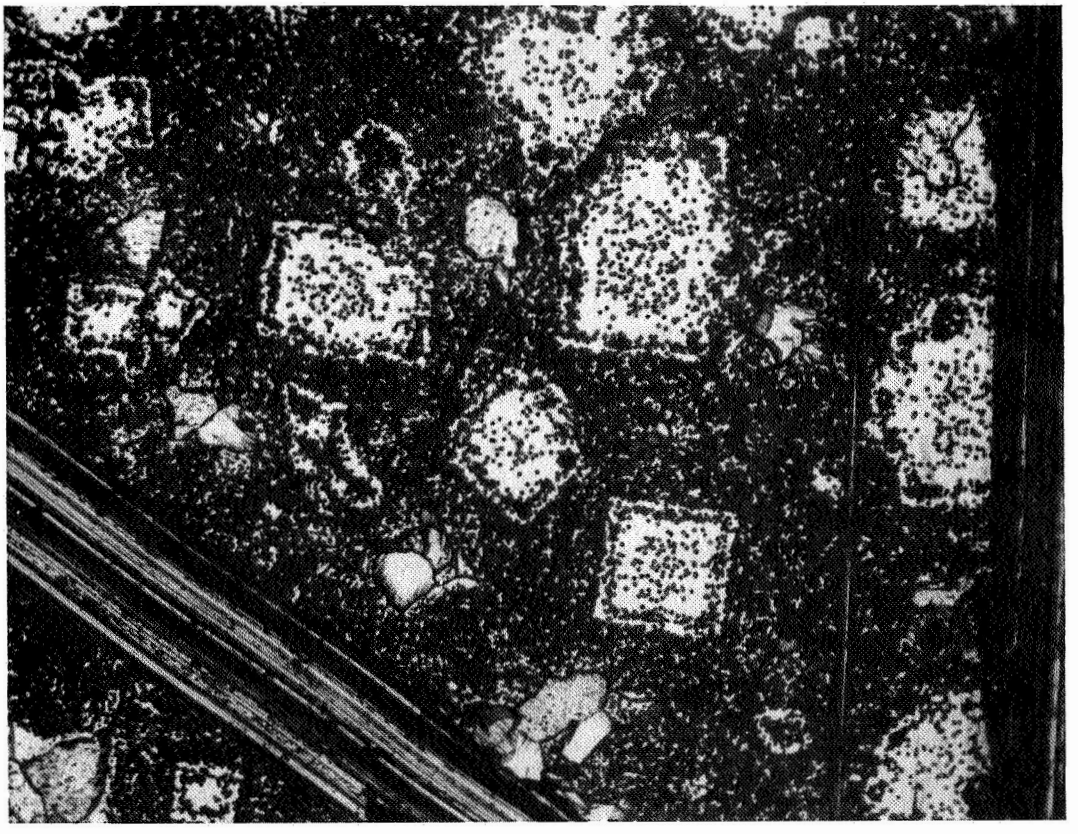

Figure V-9. Section parallel to plane of deposit through WF4C' showing dark-etching zones in each grain. (225X)

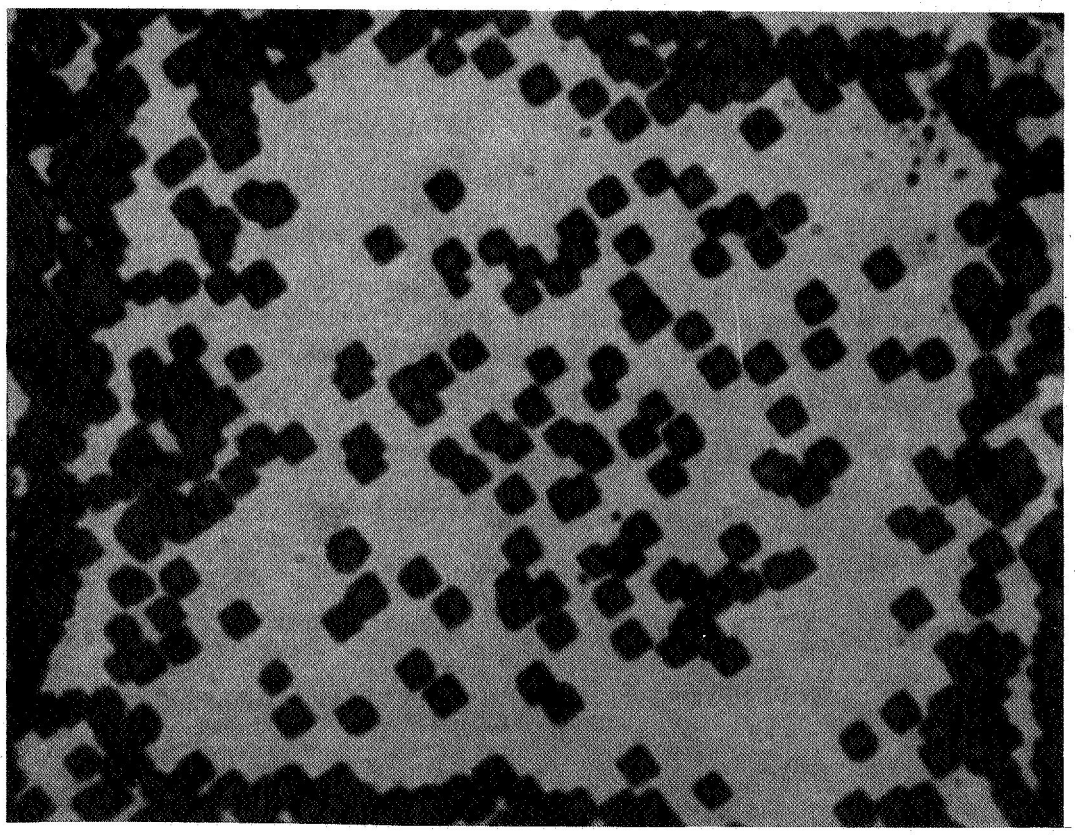

Figure V-10. Detail from Figure V-9, showing that dark etching zone has sides making 45° angle with etch pits. (1620X)

along ⟨100⟩ directions;[2] therefore, the dark-etching zone has edges in ⟨110⟩ directions, and the pyramid surfaces are {111} planes.

D. X-RAY STUDIES

Further x-ray data were obtained by the method previously reported and are presented here in the form of pole figures.

Considerable difficulty was experienced in examining samples of chloride material, because even mild heat treatment produced grain growth to the point that the region of the sample illuminated by the x-rays contained only a few large grains. The effect of this was to produce a highly irregular curve of intensity versus tilt angle α lacking symmetry about $\alpha = 0$ and composed of a few large, randomly distributed peaks. Such raw-data curves were not reduced to pole figures because it was clear that the pole figure would consist of a few steps instead of the smooth convex curve which can characterize the material. This problem was found with specimens WC2, WC3 and WC5, for which heat treatments varied from 6 hours at 1800°C to 1 hour at 2230°C.

Chloride material in the as-received condition gave the pole figure in Figure V-11, showing a fairly strong preferred orientation, but one much less strong than that of fluoride material in the same condition (Figure V-27 of the first quarterly report).

After 1.2 hours at 2230°C, specimen WC4B gave the curve in Figure V-12, for the unground top surface. Comparison of this with Figure V-11 indicates relatively slight changes, presumably associated with the changes found in the grain structure (see note at end of chapter).

[2] This confirms the conclusion of I. Berlec, J. Appl. Phys. 33:198 (1962).

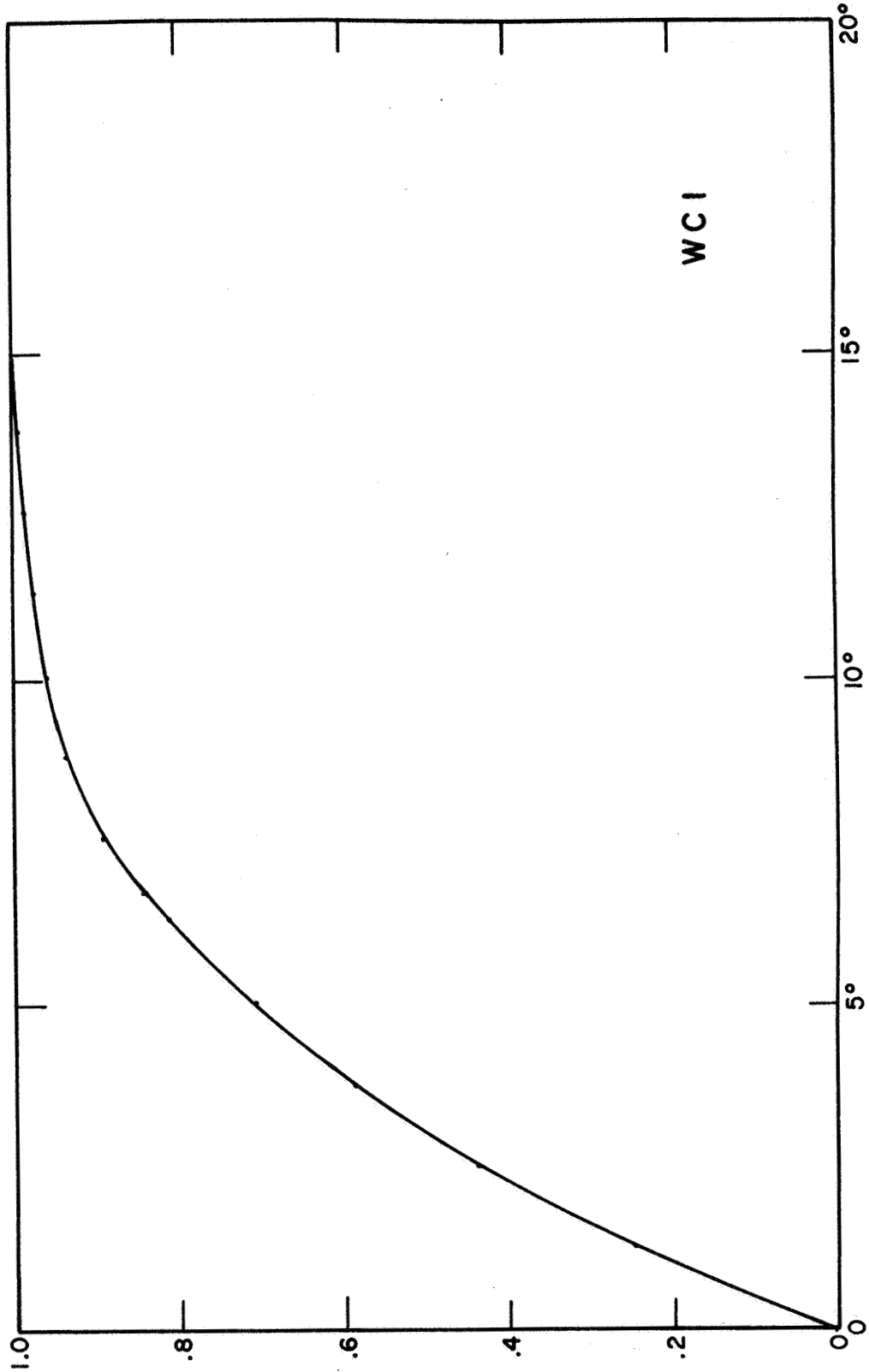

Figure V-11. Pole figure for WC1, as received.

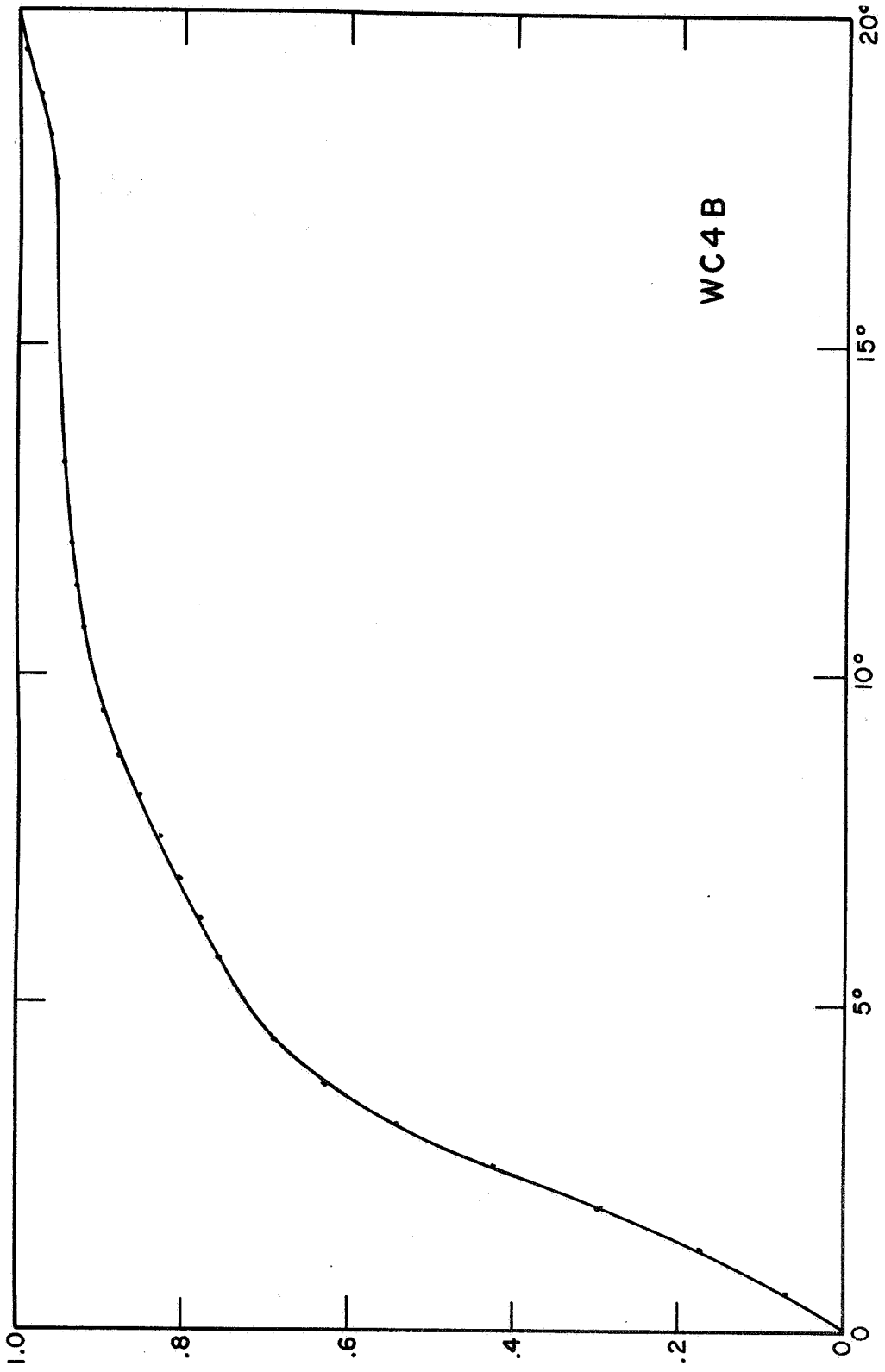

Figure V-12. Pole figure for WC4B, after 1.2 hours at 2230°C.

The sample of fluoride material examined in the as-received condition, WF, whose pole figure was Figure V-27 in the first quarterly report, was re-examined to determine the instrumental error on a sample believed to be homogeneous. The resulting curve superimposed on the original curve with a maximum error of 0.25° (at small α) and an error of less than 0.1° over most of the curve.

Sample WF4 was examined in various conditions, and the resulting pole figures for heat treatments, all at 1800°C, of 6, 30, and 100 hours on the ground surface are shown in Figure V-13. Corresponding curves for the region of WF4 electropolished for metallographic purposes are shown in Figure V-14. Each of these figures indicates that very little change in spatial distribution of ⟨100⟩ axes occurs, despite considerable changes in the microstructure, shown in Figures V-2 through V-4. Together they indicate the large degree of disordering which accompanies grinding a surface, and which is not eliminated by 1800° heat treatment, but is eliminated by electropolishing.

This observation is supported by the pole figures in Figure V-15, for an as-deposited surface subject to several heat treatments of increasing severity. The grain structure of fluoride material changes with heat treatment, but the spatial distribution of ⟨100⟩ axes does not change correspondingly.

E. CONCLUSIONS

Changes in the microstructure of fluoride vapor deposits are not necessarily accompanied by changes in the preferred orientation, as revealed by pole figures. Difficulties in obtaining pole figure data from chloride material prevent us from establishing the same conclusion definitely for that material, but it is probably also true there.

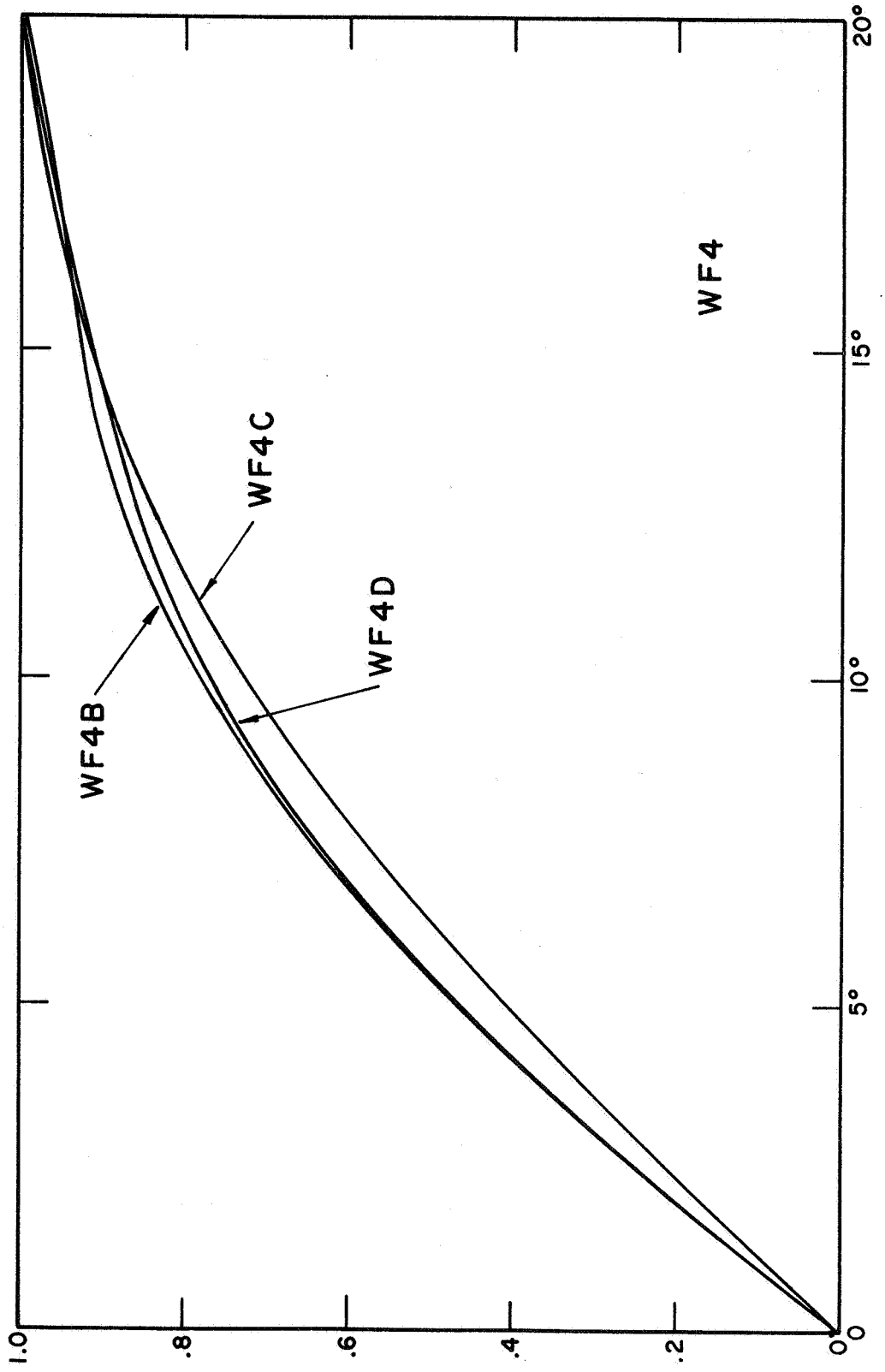

Figure V-13. Pole figures for WF4B, C, D after 6 hours, 30 hours, and 100 hours at 1800°C.

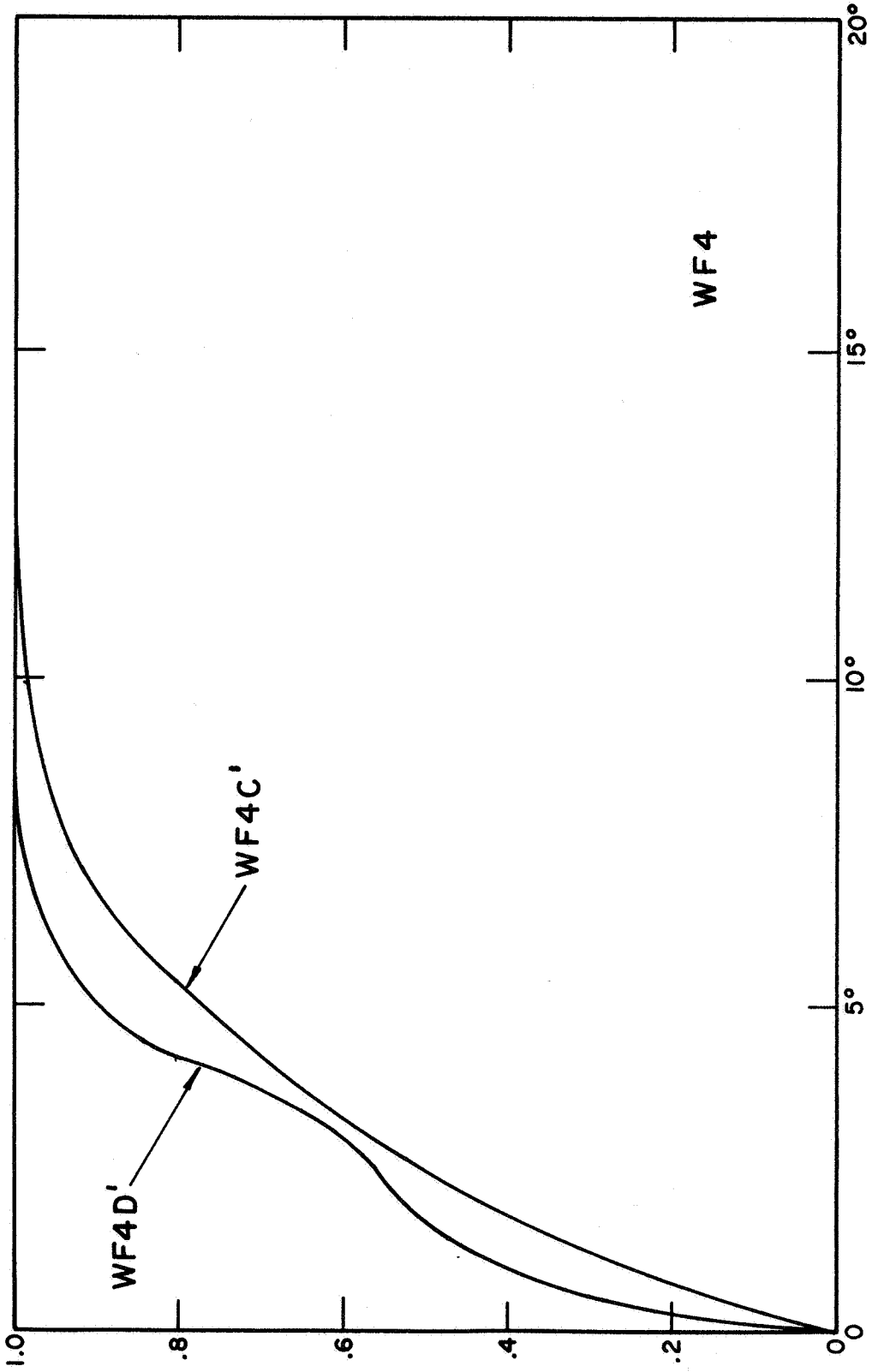

Figure V-14. Pole figures for WF4C' and D' after 30 hours and 100 hours at 1800°.

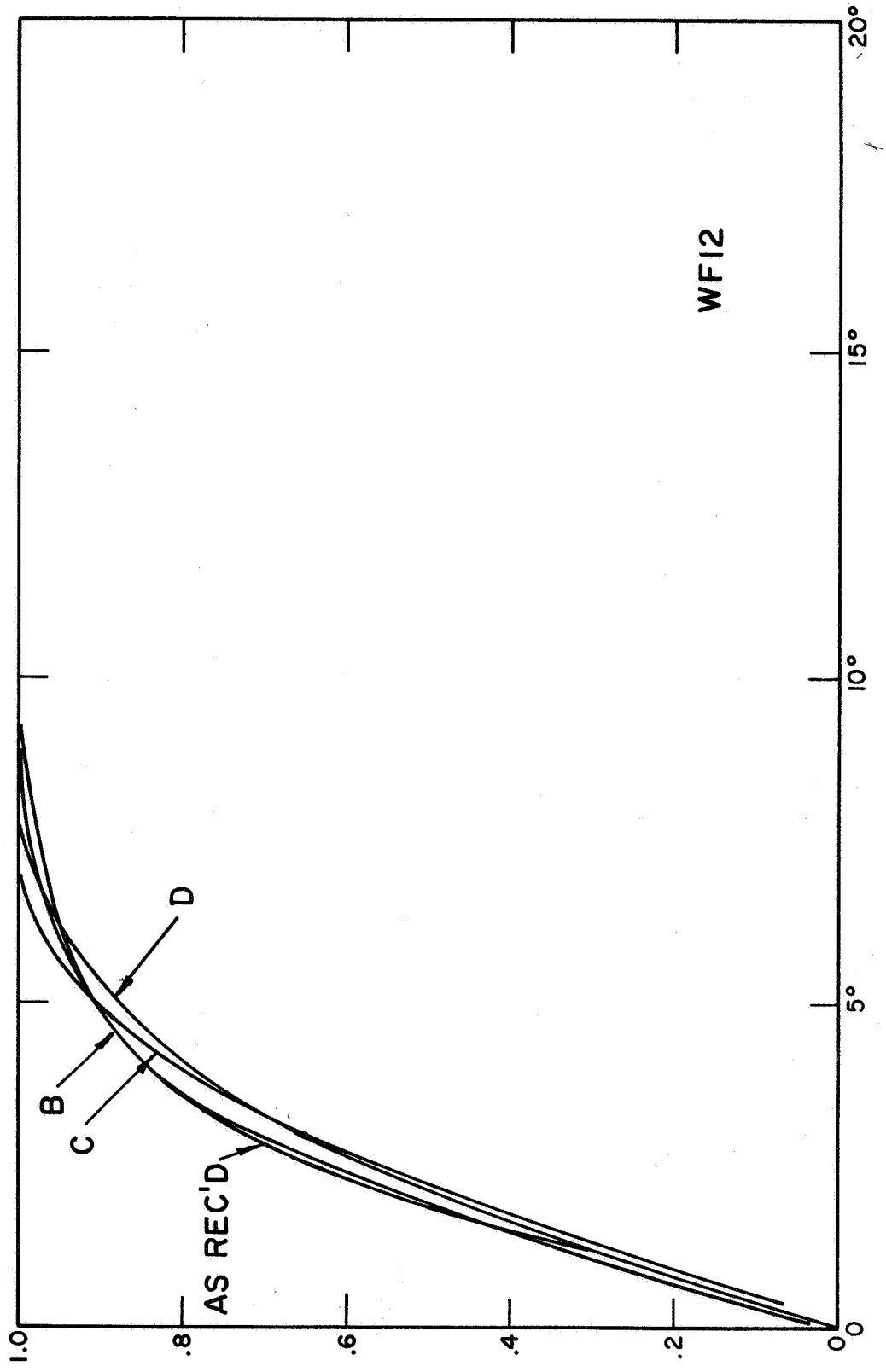

Figure V-15. Pole figures for WF12 - as received and after 1 and 6 hours at 2000° and 1 hour at 2230°C.

Note: An error was made in the captions of figures in Chapter V of the First Quarterly Report on this program, Report TE4092/3-123-68 for the period ending 4 March 1968. The three half-tone figures printed on page V-23 should be associated with the captions printed on pages V-25 to V-27, while the figures on these latter pages correspond to the captions printed on V-23. Thus the changes mentioned above in connection with Figures V-11 and V-12 of this report are in fact to be seen in the first two figures printed on page V-23 of the previous quarterly report.